ARTICLE

The RNA exosome nuclease complex regulates human embryonic stem cell differentiation

Cedric Belair[1,2], Soyeong Sim[1,2], Kun-Yong Kim[3], Yoshiaki Tanaka[3], In-Hyun Park[3], and, and Sandra L. Wolin[1,2]

A defining feature of embryonic stem cells (ESCs) is the ability to differentiate into all three germ layers. Pluripotency is maintained in part by a unique transcription network that maintains expression of pluripotency-specific transcription factors and represses developmental genes. While the mechanisms that establish this transcription network are well studied, little is known of the posttranscriptional surveillance pathways that degrade differentiation-related RNAs. We report that the surveillance pathway mediated by the RNA exosome nuclease complex represses ESC differentiation. Depletion of the exosome expedites differentiation of human ESCs into all three germ layers. LINE-1 retrotransposons and specific miRNAs, lncRNAs, and mRNAs that encode developmental regulators or affect their expression are all bound by the exosome and increase in level upon exosome depletion. The exosome restrains differentiation in part by degrading transcripts encoding FOXH1, a transcription factor crucial for mesendoderm formation. Our studies establish the exosome as a regulator of human ESC differentiation and reveal the importance of RNA decay in maintaining pluripotency.

Introduction

Embryonic stem cells (ESCs), which derive from the inner cell mass of the blastocyst, are able to self-renew indefinitely while maintaining the ability to differentiate into all three germ layers (Thomson et al., 1998). Many mechanisms that underlie these unique features have been studied extensively. Pluripotency is controlled by a network of transcription factors that includes OCT4, NANOG, and SOX2 (De Los Angeles et al., 2015). This stem cell–specific transcription factor network is associated with a less condensed "open" chromatin state that is thought to allow rapid changes in gene expression upon differentiation (Gaspar-Maia et al., 2011). Open chromatin is associated with elevated levels of chromatin-remodeling factors and increased diversity of nascent RNAs relative to differentiated cells (Efroni et al., 2008; Fort et al., 2014). In addition, transcripts from many repetitive elements, including retrotransposons such as the long interspersed nuclear elements (LINEs) and short interspersed nuclear elements, are present at increased levels (Efroni et al., 2008; Santoni et al., 2012). Thus, ESCs must balance the need to keep many genes transcriptionally competent with the need to protect themselves from deleterious consequences of promiscuous transcription.

Several mechanisms contribute to reducing levels of unwanted and potentially harmful RNAs in ESCs. The chromatin surrounding the transcription start sites (TSSs) of many developmental regulators contains active and repressive histone modifications, a "bivalent" state that may both silence these genes and promote their activation during development (Bernstein et al., 2006). RNA interference contributes to epigenetic silencing of centromeric repeats in mouse ESCs (Kanellopoulou et al., 2005). The proteasome removes preinitiation complexes from tissue-specific promoters (Szutorisz et al., 2006). However, the role of surveillance pathways in degrading differentiation-related and deleterious RNAs is poorly understood. Although in human ESCs (hESCs), down-regulation of the nonsense-mediated decay (NMD) pathway promotes differentiation into endoderm (Lou et al., 2016), the RNA targets responsible were not identified. The roles of other RNA surveillance pathways have not been investigated in hESCs.

The RNA exosome, a multiprotein nuclease complex, is the central effector of a major RNA surveillance pathway in eukaryotes (Zinder and Lima, 2017; Ogami et al., 2018). The core exosome consists of nine subunits that form a hexameric ring topped by three RNA-binding subunits. In human cells, the core exosome lacks catalytic activity, which is conferred by three associated nucleases that differ based on subcellular location (Tomecki et al., 2010). The major catalytic subunit in nucleoli is

[1]Department of Cell Biology, Yale School of Medicine, New Haven, CT; [2]RNA Biology Laboratory, Center for Cancer Research, National Cancer Institute, Frederick, MD; [3]Department of Genetics, Yale Stem Cell Center, Yale School of Medicine, New Haven, CT.

Correspondence to Sandra L. Wolin: sandra.wolin@nih.gov; C. Belair, S. Sim, and S.L. Wolin's present address is RNA Biology Laboratory, Center for Cancer Research, National Cancer Institute, Frederick, MD.

the 3′ to 5′ exoribonuclease EXOSC10 (also called hRRP6), while the nucleoplasmic exosome also contains DIS3 (hRRP44), which has both 3′ to 5′ exoribonuclease and endonuclease domains. The cytoplasmic exosome contains DIS3 or DIS3L, a related 3′ to 5′ exoribonuclease (Tomecki et al., 2010). The exosome has been best studied in yeast, where it degrades aberrant pre–ribosomal RNAs (rRNAs), pre-tRNAs, small nucleolar RNAs (snoRNAs), small nuclear RNAs (snRNAs), antisense RNAs, and "cryptic unstable transcripts" that arise from bidirectional transcription from RNA polymerase II promoters. The exosome is also required for 3′ maturation of 5.8S rRNA and many snoRNAs and contributes to mRNA decay. Many of the same RNAs are targets in human cells (Morton et al., 2018; Ogami et al., 2018).

Studies of mammalian progenitor cells support a role for the exosome in maintaining these cells in the undifferentiated state. Depletion of the EXOSC9 subunit from human epidermal progenitors results in decreased proliferation, premature differentiation, and loss of epidermal tissue (Mistry et al., 2012). The exosome promotes epidermal progenitor cell self-renewal and prevents differentiation by degrading mRNA encoding the GRHL3 transcription factor. Similarly, depleting EXOSC8 and EXOSC9 subunits from mouse erythroid precursors results in increased mature erythroid cells (McIver et al., 2014). However, progenitor cells differ from ESCs in that they are committed to a specific developmental program and undergo only a few divisions before differentiating. Despite the importance of hESCs to regenerative medicine and the need to understand the mechanisms by which they differentiate into specific lineages, the role of the exosome in regulating hESC pluripotency has not been explored.

Here, we determine the role of the exosome in maintaining the unique properties of hESCs. We show that the exosome restrains differentiation of hESCs into endoderm, mesoderm, and ectoderm. Consistent with a key role in maintaining pluripotency, down-regulation of exosome function occurs early in differentiation. We identify roles for the exosome in decreasing the levels of potentially active LINE-1 RNAs and reducing levels of specific mRNAs and noncoding RNAs (ncRNAs) that either encode key developmental regulators or regulate their expression. The exosome represses induction of mesendoderm (ME), the precursor to mesoderm and endoderm, by degrading pre-mRNA encoding forkhead box protein H1 (FOXH1), a critical transcription factor. Our studies establish the exosome as a novel regulator of hESC differentiation.

Results

Strategy for depleting the RNA exosome

We used piggyBac transposons (Ding et al., 2005) to generate hESC lines that stably express doxycycline-inducible shRNAs against mRNA encoding the core EXOSC3 subunit (Fig. 1 A). We targeted EXOSC3 (hRRP40), since its depletion destabilizes other subunits, including catalytic subunits EXOSC10 and DIS3L (Tomecki et al., 2010), allowing efficient reduction of activity. After selecting clonal cell lines, we evaluated depletion by Western blotting. Maximal depletion occurred by 5 d in doxycycline, resulting in 70% reduction in EXOSC3 (Fig. 1 B). As

described previously (Tomecki et al., 2010), EXOSC10 also decreased (Fig. 1 B). Depletion reduced exosome function, as promoter upstream transcripts (PROMPTs), short-lived transcripts upstream of RNA polymerase II promoters (Preker et al., 2008), and the 7S precursor to 5.8S rRNA (Mitchell et al., 1997) accumulated. Maximal accumulation of both RNAs occurred by 5 d in doxycycline, and the RNAs remained elevated at 7 d (Fig. 1, C and D).

We analyzed the effects of exosome depletion on hESC proliferation and expression of pluripotency markers. After 5 or 7 d in doxycycline (Figs. 1 E and S1 A), the cell cycle of EXOSC3-depleted cells was similar to that of control cells. No major effects on colony size were observed (Fig. 1 F), although some colonies expressing both EXOSC3 and control nonsilencing shRNAs (shNS) showed minor morphological changes after 7 d (Fig. 1 F, arrows), which may represent a nonspecific doxycycline effect. No differences in viability were detected after 5 or 7 d of EXOSC3 depletion (Fig. S1 B). The lack of strong effects on viability, at least during the time examined, is consistent with a study in which EXOSC3 was depleted from human HeLa cells (Tomecki et al., 2010). Levels of mRNAs encoding the pluripotency markers OCT4, NANOG, and SOX2 were unchanged upon EXOSC3 depletion (Fig. S1 C). Experiments in which we stained hESCs to detect the pluripotency marker alkaline phosphatase also did not reveal differences between control and exosome-depleted cells (Fig. S1 D).

The exosome restrains hESC differentiation

Although the levels of mRNAs encoding pluripotency markers were unaffected in EXOSC3-depleted hESCs, we detected increased levels of mRNA encoding EOMES, a transcription factor required for endoderm formation (Teo et al., 2011; Fig. S2 A). We also detected slightly increased *MIXL1* mRNA, a mesoderm marker, although this did not reach statistical significance (Fig. S2 A). To explore a role for the exosome in curtailing differentiation, we used siRNAs directed against other sites on *EXOSC3* mRNA to deplete the exosome. Depletions with either pooled or individual siRNAs were slightly more effective than shRNA depletion, resulting in 75% reduction with pooled siRNAs and one of the two individual siRNAs (siEXOSC3-2; Fig. 2 A). With these siRNAs, PROMPTs increased up to sixfold, compared with the four- to fivefold increases seen with shRNAs (Figs. 2 B and S2 B). Importantly, mRNAs encoding MIXL1, GATA4, and DLX5, markers of mesoderm, endoderm, and ectoderm, respectively, all increased in siEXOSC3-treated cells (Figs. 2 B and S2 B).

To further assess this role of the exosome, we allowed EXOSC3-depleted hESCs to differentiate into embryoid bodies (EBs), 3D structures that contain all three germ layers (Brickman and Serup, 2017). After culturing in doxycycline to deplete EXOSC3, hESCs were induced to differentiate into EBs. We used our stable shRNA-expressing cell lines for EB formation, since by culturing in doxycycline, we could maintain shRNA expression during differentiation. After 5 d of differentiation, EXOSC3-depleted EBs expressed mRNAs encoding early ectoderm (DLX5), mesoderm (MIXL1, EOMES, and TBXT), and endoderm markers (GATA4 and SOX17) at 2.5- to 15-fold higher levels than control cells (Figs. 2 C and S2 C). Examination at earlier times revealed that *EOMES* mRNA was
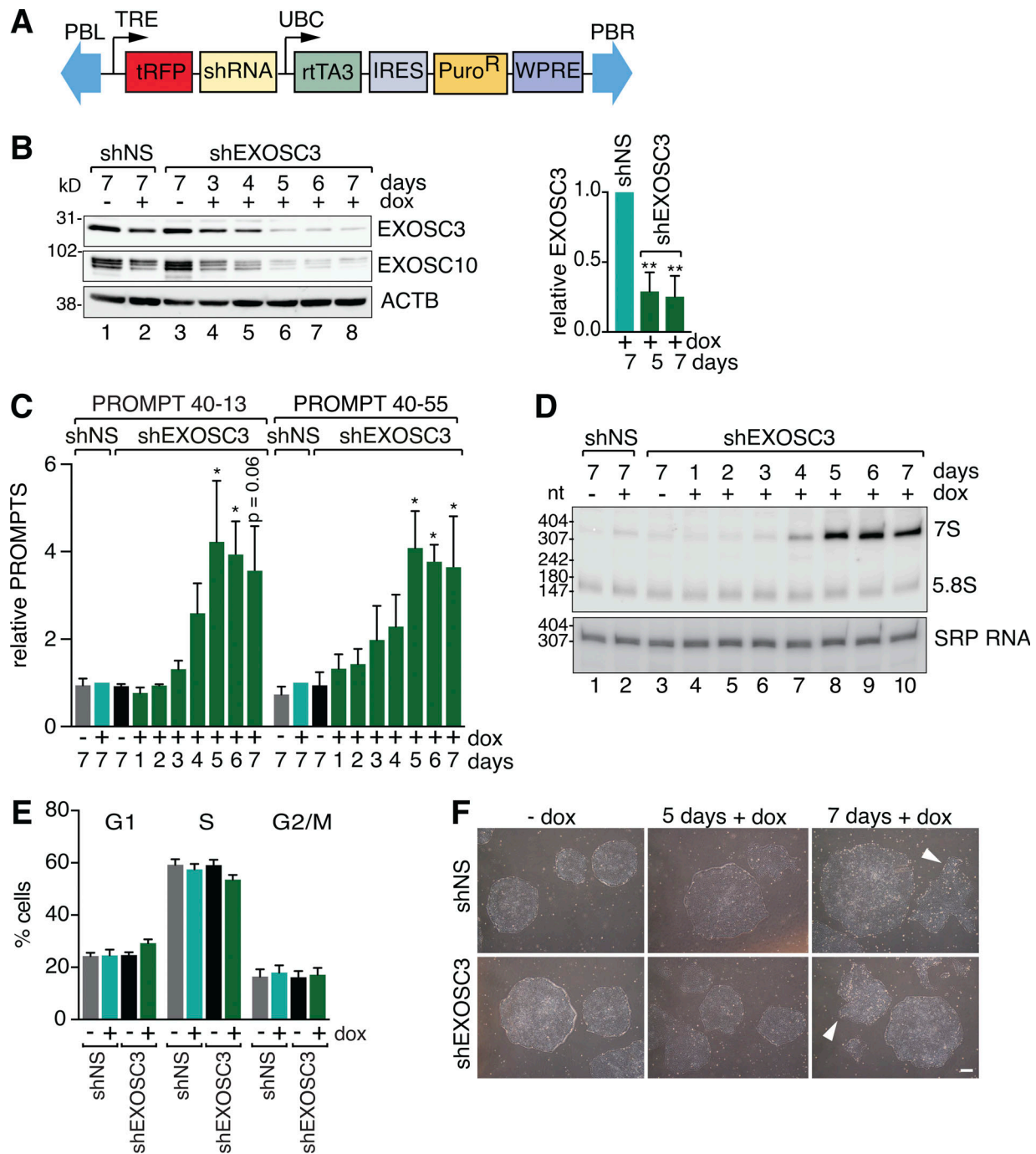
Figure 1. **Strategy for exosome depletion. (A)** Construct for EXOSC3 depletion. The tetracycline response element (TRE) drives expression of turboRFP and EXOSC3 shRNA. The ubiquitin C (UBC) promoter drives expression of the rtTA3 transactivator 3, an internal ribosome entry site (IRES) and a puromycin resistance marker (Puro^R). The woodchuck hepatitis posttranscriptional regulatory element (WPRE) enhances expression. The construct is flanked by left and right piggyBac repeat termini (PBL and PBR, respectively). **(B)** After growing hESCs expressing shEXOSC3 (lanes 3–8) or control shRNAs (shNS; lanes 1 and 2) with (+) or without (–) doxycycline for the indicated days, lysates were subjected to immunoblotting. ACTB, loading control. Right: EXOSC3 quantitation. Data are mean ± SEM ($n = 3$) compared with shNS cells in doxycycline and normalized to ACTB. **(C)** RNA from shEXOSC3- or shNS-expressing cells grown with or without doxycycline was subjected to RT-qPCR to detect two PROMPTs. Normalization was to *ACTB*. Data are mean ± SEM ($n = 3$) relative to shNS cells in doxycycline. **(D)** RNA from shRNA-expressing cells grown with or without doxycycline was subjected to Northern blotting to detect the 7S precursor to 5.8S rRNA. Signal recognition particle RNA (SRP RNA), loading control. **(E)** Cell cycle analyses of shEXOSC3- and shNS-expressing hESCs grown for 5 d with or without doxycycline. BrdU incorporation was measured by flow cytometry. Data are mean ± SEM ($n = 5$). **(F)** Morphology of hESC colonies expressing EXOSC3 or nonsilencing shRNAs grown with or without doxycycline (dox) for 5 or 7 d. Arrowheads show colonies with minor morphological changes. Scale bar, 220 µm. P values were calculated with one-way ANOVA. *, $P < 0.05$; **, $P < 0.01$.
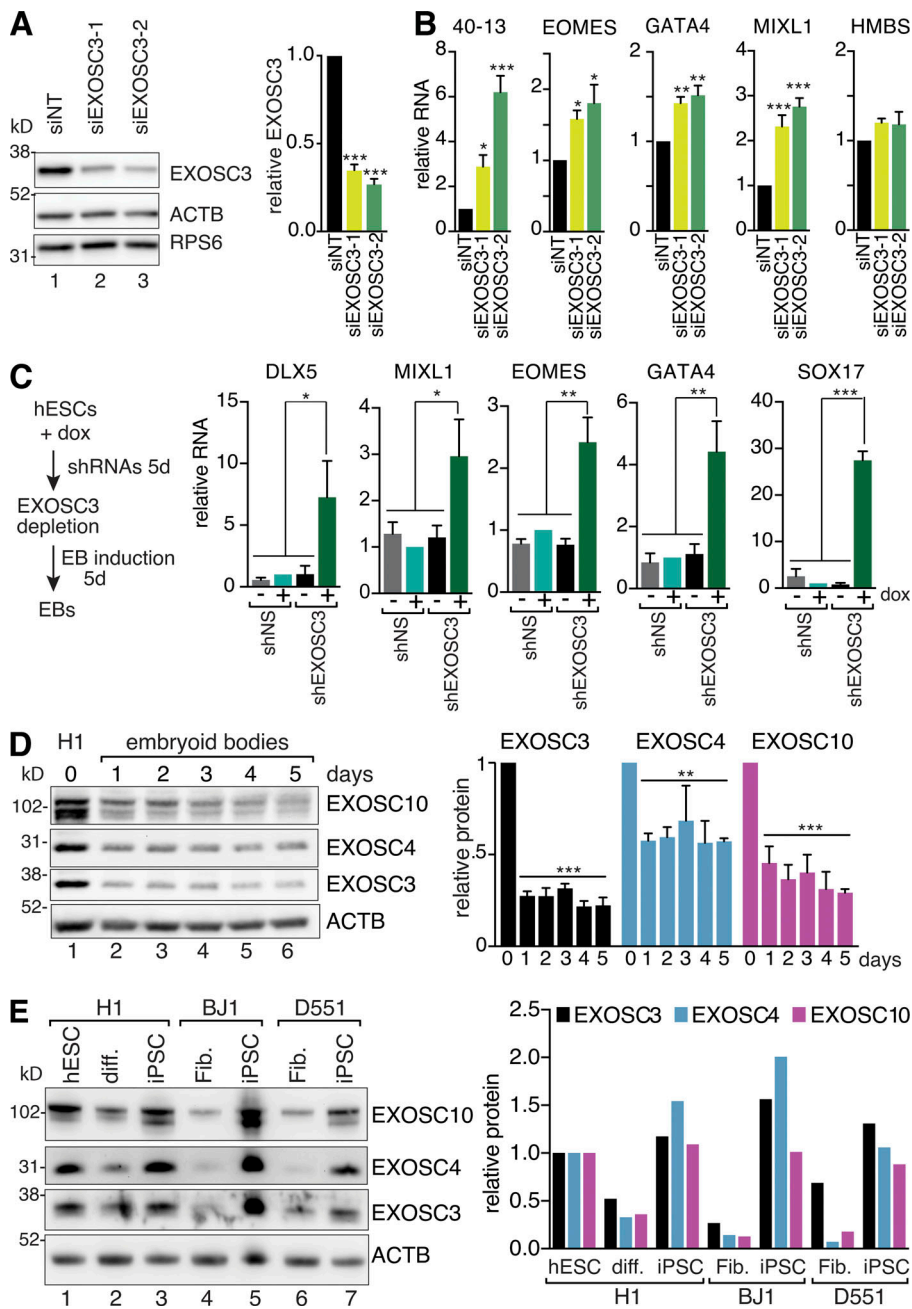
Figure 2. **The exosome restrains hESC differentiation. (A)** After transfecting hESCs with nontarget (siNT) or two siEXOSC3 RNAs, lysates were subjected to immunoblotting to detect EXOSC3. ACTB and RPS6 are loading controls. Right: EXOSC3 quantitation. Data are mean ± SEM ($n = 3$), normalized to RPS6. **(B)** After treating hESCs with siNT or siEXOSC3 RNAs, the indicated RNAs were measured by RT-qPCR. *HMBS* encodes a housekeeping enzyme, hydroxymethylbilane synthase. Data are mean ± SEM ($n = 4$), relative to siNT-treated cells and normalized to *ACTB*. **(C)** After growing hESCs expressing EXOSC3 or nonsilencing shRNAs with or without doxycycline for 5 d, EB formation was induced and the cells were cultured an additional 5 d. The indicated mRNAs were detected by RT-qPCR. Data are mean ± SEM ($n = 3$), relative to shNS EBs in doxycycline and normalized to *ACTB*. **(D)** EXOSC10, EXOSC4, and EXOSC3 levels in WT H1 cells (lane 1) and the corresponding EBs after 1–5 d of induction were assessed by immunoblotting (lanes 2–6). Right: Quantitation. Proteins were normalized to ACTB. Data are mean ± SEM ($n = 3$) relative to day 0. **(E)** Levels of the indicated subunits were compared by immunoblotting H1 hESCs (lane 1), three primary somatic cell lines (H1 differentiated cells, BJ1 neonatal foreskin fibroblasts [BJ1] and Detroit 551 [D551] fetal cells; lanes 2, 4, and 6), and iPSCs derived from each cell line (lanes 3, 5 and 7). Right: Quantitation of the blot shown ($n = 1$). P values were calculated with one-way ANOVA. *, $P < 0.05$; **, $P < 0.01$; ***, $P < 0.001$.

elevated in EXOSC3-depleted EBs within 2 d of differentiation, with significant changes by day 4 (Fig. S2 D). Similar increases in mRNAs encoding differentiation markers (MIXL1, EOMES, GATA4, SOX17, and PAX6, an early ectoderm marker) were observed in EBs formed from a second hESC line expressing shRNAs against EXOSC3 (Fig. S2 E).

As our results suggested that the exosome inhibits hESC differentiation, we determined if down-regulation of this nuclease complex occurs during differentiation of WT hESCs. We compared the levels of several subunits in H1 hESCs (which are male) and their corresponding EBs by immunoblotting. Within 1 d of differentiation, EXOSC3, EXOSC4, and EXOSC10 proteins decreased (Fig. 2 D). Similar changes were observed when EBs were formed from a second line, female H9 hESCs (Fig. S2 F).

Down-regulation occurred after transcription as the mRNAs encoding the nine core subunits and three catalytic subunits did not decrease (Fig. S2 G).

To determine if high levels of exosome subunits correlate with the pluripotent state, we examined reprogramming of differentiated cells into induced pluripotent stem cells (iPSCs). Comparison of differentiated cells derived from H1 hESCs (Park et al., 2008) with the resulting iPSCs revealed that EXOSC3, EXOSC4, and EXOSC10 all increased at least twofold upon reprogramming (Fig. 2 E). All three subunits also increased 2–15-fold when two primary human fibroblast lines (BJ1 and Detroit 551) were reprogrammed (Fig. 2 E), consistent with reports that *EXOSC1*, *EXOSC2*, *EXOSC7*, *EXOSC9*, and *DIS3* mRNAs are up-regulated early in reprogramming of

fibroblasts to iPSCs (Polo et al., 2012). Our results reveal that the exosome restrains differentiation of hESCs and support a model in which elevated exosome levels are important for maintaining pluripotency.

HITS-CLIP in hESCs identifies new exosome targets

To identify RNAs that are direct exosome targets, we performed in vivo cross-linking. We cross-linked proteins to their targets with UV (254 nm) followed by immunoprecipitation and HITS-CLIP (high-throughput sequencing of RNA isolated by cross-linking immunoprecipitation; Licatalosi et al., 2008). We used antibodies against EXOSC3, part of the exosome cap, and EXOSC4, part of the hexameric ring. Nonimmune IgG was a control (Fig. S3 A). More EXOSC4 tags were recovered than EXOSC3 tags (2.3 million vs. 1.5 million) and were derived from a greater variety of RNAs (Fig. 3 A), possibly because RNA substrates make multiple contacts with EXOSC4 (Weick et al., 2018). Both 45S pre-rRNA and 5S rRNA were prominent targets, consistent with a study in yeast (Schneider et al., 2012). Some tags derived from known pre-rRNA targets, such as the 5′ external transcribed spacer (5′ETS) and internal transcribed spacers 1 and 2 (Fig. 3, B–D). In addition to other known targets, such as mRNAs, introns, and ncRNAs, we obtained tags from repeat element transcripts and from mitochondrial rRNAs (mt-rRNAs). Levels of all tags were strongly reduced in the control sample. As expected, EXOSC3 and EXOSC4 tags were enriched for the cross-linking–induced mutation sites (Moore et al., 2014) that occur during reverse transcription across the residual cross-linked oligopeptide (Fig. 3, E and F).

Since many exosome targets are expected to be short lived, we also used 4-thiouridine to label nascent RNA, followed by cross-linking with UV (365 nm) and immunoprecipitation (Hafner et al., 2010). Since HITS-CLIP and PAR-CLIP (photoactivatable ribonucleoside-enhanced cross-linking and immunoprecipitation) rely on different cross-linking chemistries, use of both protocols recovers a wider range of targets (Castello et al., 2012). To maximize our yield of cross-linked RNAs, we used the iCLIP (individual nucleotide resolution cross-linking and immunoprecipitation) protocol (Huppertz et al., 2014), which recovers cDNAs that truncate prematurely at the site of the cross-link. Using this PAR-iCLIP protocol with antibodies to EXOSC4, the fraction of tags that mapped to the ribosomal DNA and 5S rRNAs declined, while the fraction of repeat transcripts and ncRNAs increased (Fig. 3 A). As expected for a protocol that recovers newly made RNAs, tags derived from pre-45S rRNA spacers were abundant in PAR-iCLIP (Fig. 3, C and D).

Since the exosome functions with oligo(A) polymerases to degrade some RNAs (Zinder and Lima, 2017; Ogami et al., 2018), we examined tags for nontemplated A tails. Although known targets such as the 5′ETS were present in both HITS-CLIP and PAR-iCLIP (Fig. 3, G and H), 81% of the EXOSC3 and 73% of the EXOSC4 tags with A tails in HITS-CLIP mapped to 16S mt-rRNA, with most tags from the 3′ end (Fig. 3, G and I). This RNA is transcribed as a polycistronic precursor, with the 3′ end generated by RNase P cleavage of the downstream tRNA^{Leu}. Since most tails began after the first G of the tRNA, these RNAs may represent aberrant cleavage products (Fig. 3 I). As expected for

bona fide targets, A-tailed 16S mt-rRNAs accumulated when EXOSC3 was depleted with siRNAs (Fig. 3 J).

L1 transcripts are exosome targets

To identify the effects of exosome depletion on a transcriptome-wide scale, we sequenced rRNA-depleted RNA from shEXOSC3 and shNS-expressing cells after 5 and 7 d in doxycycline, as well as from cells grown without doxycycline. Since RNAs that increase are most likely to be direct targets, we focused on transcripts that increased >1.2-fold upon EXOSC3 depletion, compared with control cells (Table S1). As expected, known targets, such as 3′ extended forms of snRNAs, snoRNAs, and telomerase RNA (Lubas et al., 2015; Macias et al., 2015; Nguyen et al., 2015; Tseng et al., 2015), increased upon EXOSC3 depletion (Fig. S3). Although most mature ncRNAs were not strongly affected, the minor spliceosome U4atac snRNA (Tarn and Steitz, 1997) increased 2.5-fold (Fig. S3), suggesting exosome-mediated degradation of pre-U4atac could affect pre-mRNA splicing in hESCs.

Notably, transcripts derived from L1 LINEs were targets in HITS-CLIP and PAR-iCLIP (Fig. 4 A) and increased upon EXOSC3 depletion. These elements, which comprise ~17% of the genome, are the only known active autonomous retrotransposons in humans. Although full-length L1 RNA is ~6 kb, most genomic copies are truncated and/or contain inactivating mutations, and only 80–100 members of the human-specific L1Hs subfamily remain capable of retrotransposition (Beck et al., 2011). L1 RNAs were prominent targets, comprising 3.9% and 5.0% of the EXOSC4 tags in HITS-CLIP and PAR-iCLIP, respectively. Mapping the tags against a retrotransposition-competent L1Hs sequence revealed that the tags were 27- and 30-fold enriched, respectively, compared with the control (Fig. 4 B). The tags mapped throughout the RNA, including the 5′UTR (Fig. 4 C), the region most likely to be truncated (Beck et al., 2011).

In support of the hypothesis that active LINEs are exosome targets, L1Hs RNAs increased upon EXOSC3 depletion (Fig. 4 D). The increase in L1Hs RNAs was accompanied by increased ORF1, the more easily detected of the two L1-encoded proteins (Fig. 4 E, lane 5). Using quantitative RT-PCR (RT-qPCR), we confirmed that L1Hs RNAs increased in EXOSC3-depleted cells (Fig. 4 F) and that levels of other retrotransposons, such as the Alu family of short interspersed nuclear elements, were unchanged (Fig. 4 G). L1Hs RNAs also increased when siRNAs targeting other sites on EXOSC3 or the catalytic subunits were used (Fig. 4, H and I). As depleting EXOSC10 together with DIS3 resulted in accumulation of L1 RNAs to levels seen when EXOSC3 was depleted (Fig. 4 I), degradation may occur within nuclei. Although attempts to determine if exosome depletion increased retrotransposition using an engineered element were inconclusive due to the low efficiency of hESC transfection (Garcia-Perez et al., 2007), our experiments identify L1 RNAs as exosome targets.

The exosome regulates levels of specific miRNAs and long ncRNAs (lncRNAs)

Although primary miRNA transcripts (pri-miRNAs) are not known exosome targets, pri-miR-205 was bound by the exosome in HITS-CLIP and PAR-iCLIP and was up-regulated on exosome depletion (Fig. 5, A and B; and Table S1). The encoded miRNA regulates the
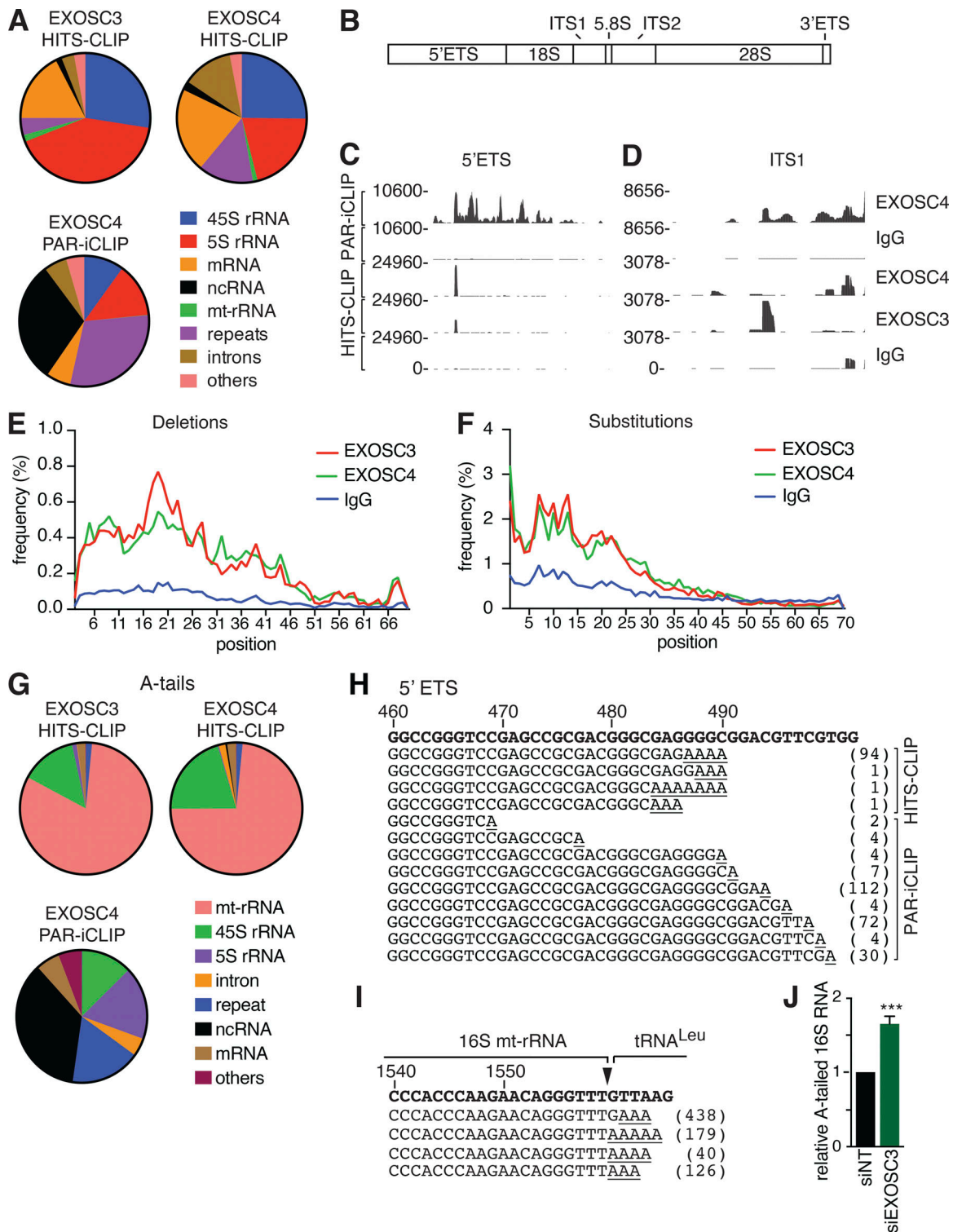
Figure 3. **HITS-CLIP identifies known and new targets of the RNA exosome. (A)** Distribution of tags from HITS-CLIP and PAR-iCLIP. **(B)** Cartoon of human ribosomal DNA, showing the 5'ETS, 18S rRNA, first internal transcribed spacer (ITS1), 5.8S rRNA, second internal transcribed spacer (ITS2), 28S rRNA, and 3'ETS. **(C and D)** HITS-CLIP and PAR-iCLIP reads mapping to the 5'ETS (C) and ITS1 (D). **(E and F)** Positions of deletions (E) and substitutions (F) in EXOSC3, EXOSC4, and IgG HITS-CLIP reads relative to the 5' ends of the reads. **(G)** Distribution of HITS-CLIP and PAR-iCLIP reads containing nontemplated A tails. **(H)** Representative adenylated reads mapping to the 5'ETS. Genomic sequence is at the top. The number of reads is in parentheses. **(I)** Adenylated reads mapping to the 16S mt-rRNA 3' end. Genomic sequence is at the top. Arrowhead, 16S mt-rRNA 3' end. The number of reads is in parentheses. **(J)** RT-qPCR quantitation of polyadenylated 16S mt-rRNA in cells treated with EXOSC3 or NT siRNAs. Data are mean ± SEM (*n* = 4), normalized to *ACTB*. P values were calculated using two-tailed unpaired *t* test. ***, P < 0.001.
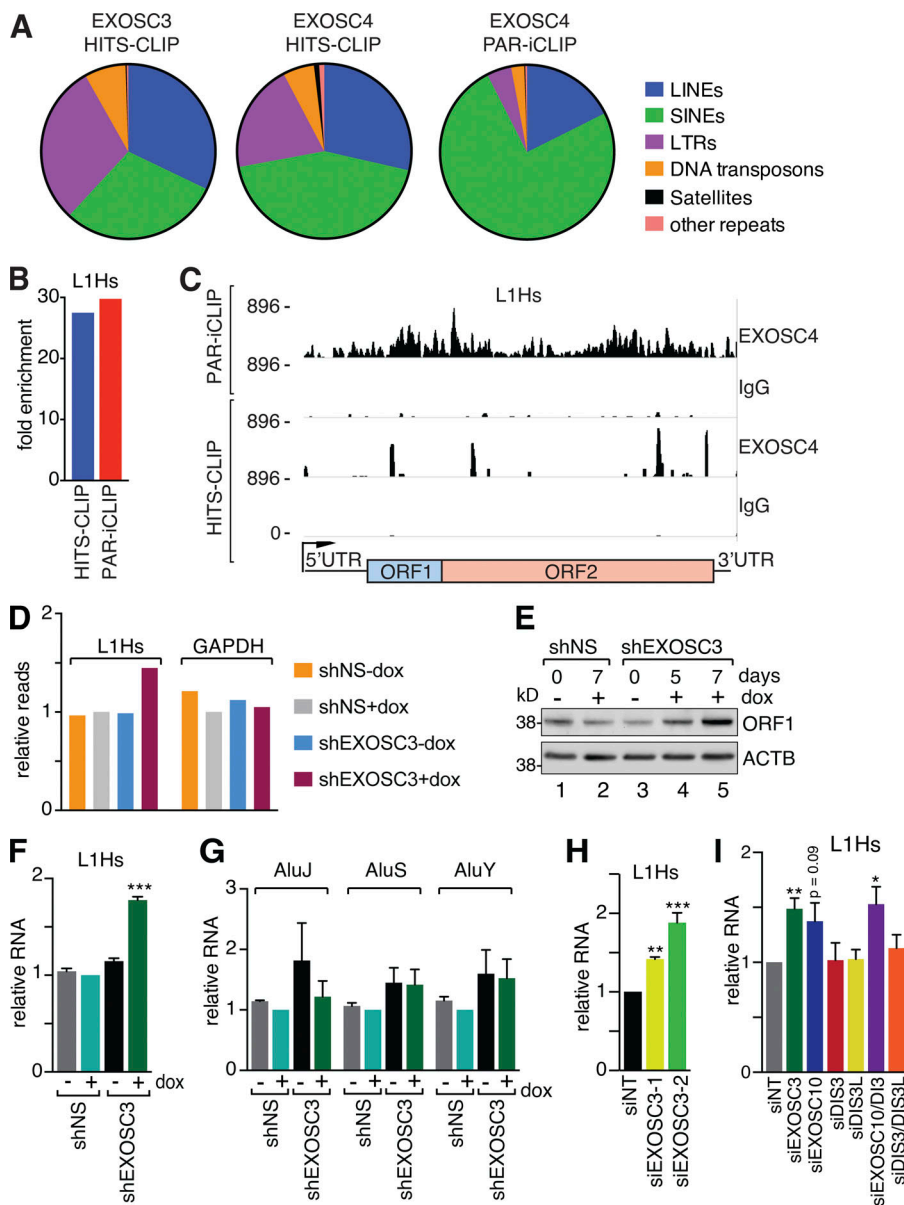
Figure 4. **The exosome reduces L1 RNA levels.** **(A)** Distribution of tags mapping to repeat elements. **(B)** Enrichment of EXOSC4 HITS-CLIP and PAR-iCLIP tags mapping to a retrotransposition-competent L1Hs element. Bars show the ratio of EXOSC4 reads compared with control IgG. **(C)** Distribution of tags mapping to a L1Hs consensus sequence. **(D)** RNA-seq reads for L1Hs elements from hESCs grown with or without doxycycline for 7 d. Read counts are normalized by the total reads in each library, relative to shNS cells in doxycycline (n = 1). **(E)** Lysates were subjected to immunoblotting to detect ORF1p. ACTB, loading control. **(F and G)** RT-qPCR analyses of L1Hs (F) or AluY, AluS, and AluJ RNA levels (G) in shNS and shEXOSC3-expressing cells grown with or without doxycycline for 7 d. Data are mean ± SEM (n = 3). Normalization was to *ACTB* relative to shNS cells in doxycycline. **(H and I)** After transfecting hESCs with individual (H) or siRNA pools (I), L1Hs RNAs were measured by RT-qPCR. Data are mean ± SEM (n = 3). Normalization was to *ACTB*, relative to siNT-transfected cells. P values were calculated with one-way ANOVA. *, P < 0.05; **, P < 0.01; ***, P < 0.001.

epithelial-to-mesenchymal transition by down-regulating the ZEB1 and ZEB2 transcriptional repressors (Gregory et al., 2008) and overexpression of miR-205 in mouse ESCs increases differentiation into extraembryonic endoderm (Li et al., 2013). The pre-miRNA spans the intron–exon junction of the MIR205 host gene (*MIR205HG*) and is cleaved from unspliced *MIR205HG* RNA (i.e., pri-miRNA), while the spliced form encodes a lncRNA. Both unspliced and spliced RNAs increased in EXOSC3-depleted hESCs (Fig. 5 B). As the mature miRNA also increased (Fig. 5 C), miR-205 levels are regulated by the exosome.

We also identified a way in which the exosome could contribute to pluripotency by modulating lncRNA levels. Several lncRNAs encoded antisense to the TSSs of coding genes were both targets and up-regulated on exosome depletion (Fig. 5 D and Table S1). Up-regulation of lncRNA loc644656 was associated with increased reads mapping to the first intron of the adjacent *ZNF143* (Fig. 5 E), which encodes a transcription factor important for mouse and hESC pluripotency (Chen et al.,

2008; Chia et al., 2010). In addition to this ESC-specific role, *ZNF143* regulates expression of many mRNAs and ncRNAs (Ngondo-Mbongo et al., 2013) and is important for establishing chromatin interactions at promoters (Bailey et al., 2015). ZNF143 levels are partly maintained by an autoregulatory loop involving an alternative TSS. When ZNF143 is high, it binds downstream of the normal TSS (TSS1), resulting in initiation in the first intron (Fig. 5 E). The resulting TSS2 mRNA is poorly translated (Ngondo and Carbon, 2014). Using siRNAs, we confirmed that exosome depletion results in decreased TSS1 mRNA, increased TSS2 mRNA, and reduced ZNF143 (Fig. 5, F and G). Our data support a model in which exosome degradation of the lncRNA regulates ZNF143 levels.

The exosome targets mRNAs with key roles in development and gene regulation

Numerous mRNAs increased upon EXOSC3 depletion (Table S1). Gene Ontology (GO) analyses revealed that many mRNAs
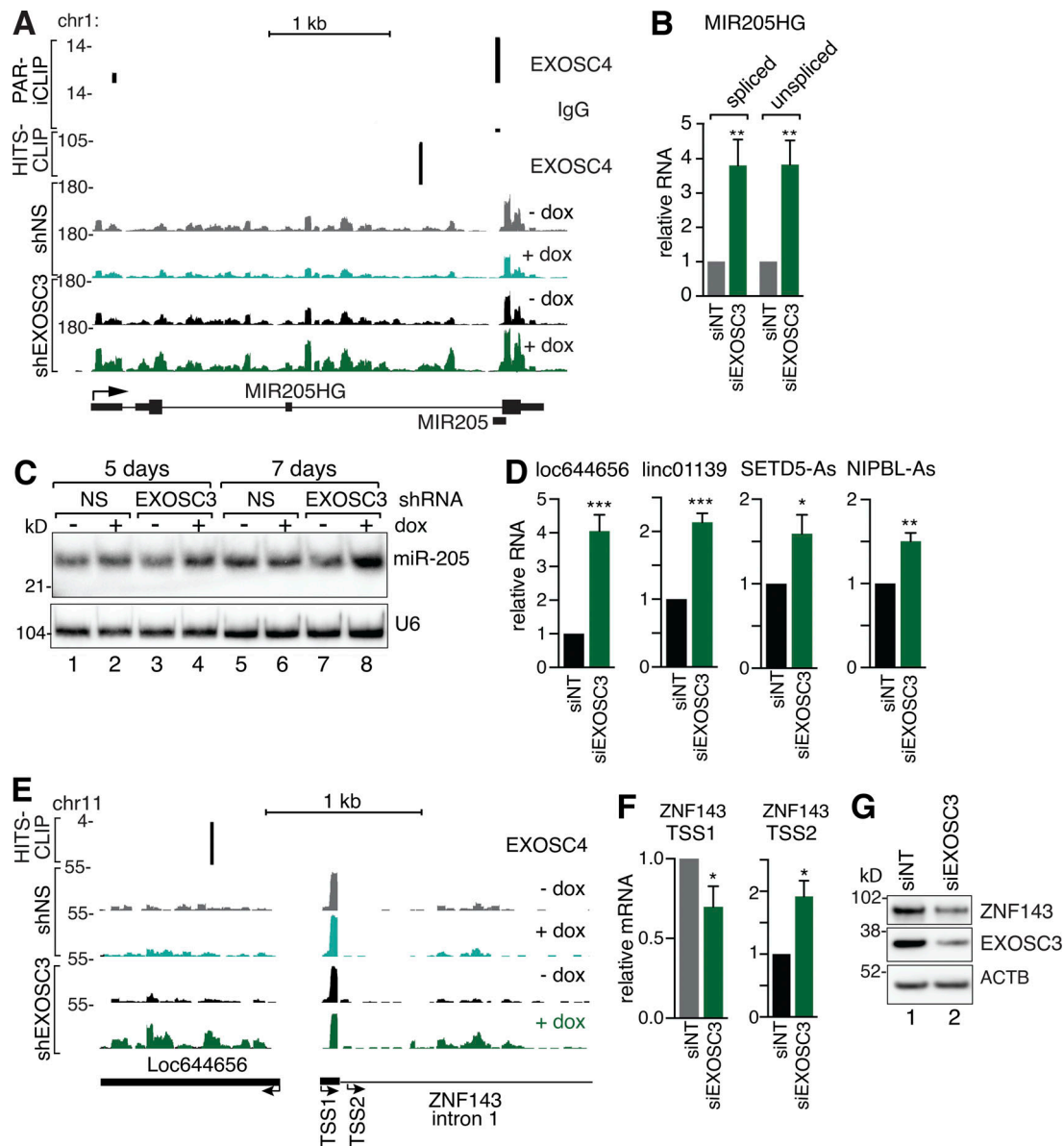
Figure 5. **The exosome regulates levels of specific pre-miRNAs and lncRNAs. (A)** EXOSC4-bound CLIP and RNA-seq reads mapping to *MIR205HG*. For RNA-seq, hESCs were grown with or without doxycycline for 7 d. **(B)** RT-qPCR analyses of *MIR205HG* transcripts in siNT- and siEXOSC3-treated cells. Data are mean ± SEM (*n* = 6). Normalization was to *ACTB*, relative to siNT cells. **(C)** RNA from shNS- (lanes 1, 2, 5, and 6) or shEXOSC3-expressing (lanes 3, 4, 7, and 8) cells grown with or without doxycycline for 5 or 7 d was subjected to Northern blotting to detect miR-205. U6 RNA, loading control. **(D)** Levels of the indicated lncRNAs were measured by RT-qPCR in hESCs transfected with siEXOSC3 or siNT RNAs. Data are mean ± SEM (*n* = 4). Normalization was to *ACTB*, relative to siNT-transfected cells. **(E)** EXOSC4-bound fragments and RNA-seq reads mapping to LOC644656 and the 5′ portion of *ZNF143*. *ZNF143* TSSs (TSS1 and TSS2) are indicated. **(F)** Transcripts from TSS1 or TSS2 were measured by RT-qPCR in siEXOSC3 or siNT-treated hESCs. Data are mean ± SEM (*n* = 4). **(G)** Levels of ZNF143 and EXOSC3 in siNT- and siEXOSC3-treated hESCs were analyzed by immunoblotting. ACTB, loading control. P values were calculated with two-tailed unpaired *t* tests. *, P < 0.05; **, P < 0.01; ***, P < 0.001.

involved in regulation of development and tissue formation increased, while genes associated with maintaining pluripotency were largely unaffected (Fig. 6, A and B). Since our CLIP experiments collectively identified >5,500 mRNAs, we focused on mRNAs that were identified by both HITS-CLIP and PAR-iCLIP as high-confidence targets (1,114 mRNAs; Fig. 6 C). Using this stringent definition, some mRNAs associated with regulation of development were both exosome targets and increased upon exosome depletion (Fig. 6 B, names in bold; and Fig. S4).

Consistent with findings that the exosome degrades pre-mRNAs and mature mRNAs (Lubas et al., 2011, 2015), introns, 3′ UTRs, and exons were all targets in HITS-CLIP and PAR-iCLIP (Fig. 6 D).

Exosome targets that encode proteins with critical roles in gene regulation and/or development included *FOXH1*, which encodes a transcription factor required for anterior–posterior patterning and endoderm development in mice and ME induction in hESCs (Labbé et al., 1998; Hoodless et al., 2001;
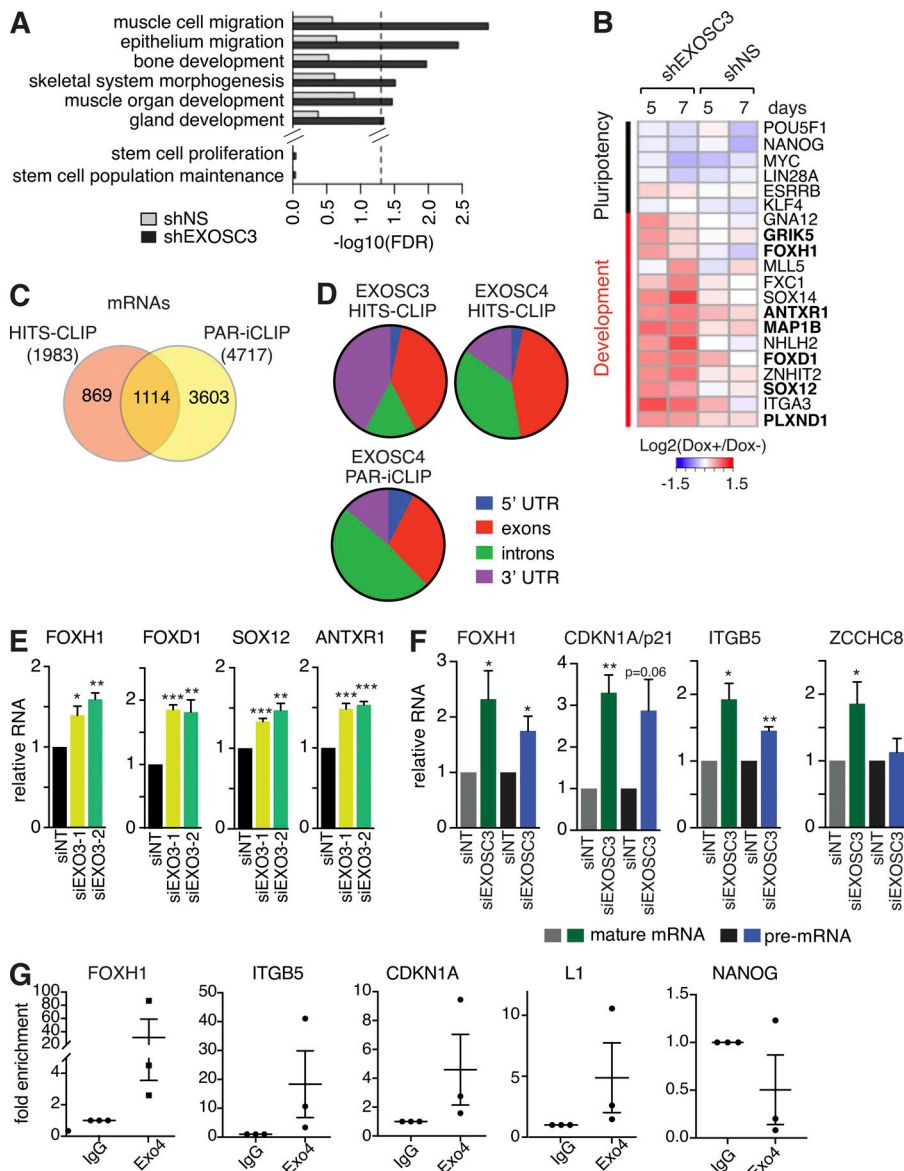
Figure 6. **Exosome targets include mRNAs with roles in development and gene regulation. (A)** Significant GO terms for differentially expressed genes after 5 and 7 d of doxycycline treatment in shNS and shEXOSC3-expressing hESCs. Dashed line, 0.05 false discovery rate cutoff. **(B)** Heat map showing expression changes of representative genes important for pluripotency and differentially expressed genes important for development. Genes in bold were exosome targets in HITS-CLIP and PAR-iCLIP. **(C)** Venn diagram showing the number of mRNAs bound by the exosome in HITS-CLIP and PAR-iCLIP, along with mRNAs identified by both techniques. **(D)** HITS-CLIP and PAR-iCLIP reads mapping to mRNA 5′ UTRs, introns, exons, and 3′ UTRs. **(E and F)** Levels of the indicated mRNAs and pre-mRNAs in hESCs transfected with individual (E) or pooled (F) siRNAs against *EXOSC3* were measured by RT-qPCR. Data are mean ± SEM (*n* = 3). Normalization was to *ACTB*, relative to siNT-treated cells. **(G)** After UV cross-linking and immunoprecipitation, levels of the indicated RNAs were measured by RT-qPCR. The fold enrichment of each RNA in anti-EXOSC4 immunoprecipitates compared with IgG controls is shown. Data are mean ± SEM (*n* = 3). P values were calculated with two-tailed unpaired *t* tests. *, $P < 0.05$; **, $P < 0.01$; ***, $P < 0.001$.

Yamamoto et al., 2001; Beyer et al., 2013); *FOXD1*, which encodes a transcription factor important for kidney and retina development (Quintero-Ronderos and Laissue, 2018); *SOX12*, which functions redundantly with *SOX4* and *SOX11* in organogenesis (Bhattaram et al., 2010); and *CDKN1A*, a known target that encodes the cyclin-dependent kinase inhibitor that regulates the G1/S transition. Using RT-qPCR, we confirmed that the mRNAs and pre-mRNAs increase when *EXOSC3* mRNA is depleted (Fig. 6, E and F; and Fig. S4). Other mRNA targets that increased upon EXOSC3 depletion encoded ITGB5, an integrin important for keratinocyte proliferation (Duperret et al., 2015), and ZCCHC8, a subunit of the nuclear exosome targeting complex that recruits the exosome to PROMPTs, pre-mRNAs, and pre-snoRNAs (Lubas et al., 2011, 2015). Both *ZCCHC8* mRNA and protein increased upon exosome depletion (Fig. S4), consistent with a possible regulatory loop in which decreased exosome activity is compensated by increases in the levels of its cofactors.

To confirm the association of these RNAs with the exosome, we performed UV cross-linking of hESCs, followed by immunoprecipitation with antibodies against EXOSC4, and analyzed RNAs in the immunoprecipitates. RNAs identified as exosome bound by both HITS-CLIP and PAR-iCLIP, including *FOXH1*, *ITGB5*, and *CDKN1A* mRNAs and L1 RNAs, were all enriched in anti-EXOSC4 immunoprecipitates compared with control immunoprecipitates, while *NANOG* mRNA, which is not a high-confidence exosome target, was not enriched (Fig. 6 G).

Exosome-mediated down-regulation of *FOXH1* mRNA represses ME induction
Since the exosome restricts hESCs from differentiating (Fig. 2), we examined which targets could potentially mediate this function. Consistent with reports that *CDKN1A* mRNA is regulated by miRNAs in ESCs (Wang et al., 2008; Dolezalova et al., 2012), we did not detect CDKN1A in EXOSC3-depleted or control hESCs, and the fraction of cells in G1 was unchanged (Fig. 1 E).

Although ZNF143 depletion was reported to reduce *NANOG* transcription in mouse ESCs and cause cells to differentiate (Chen et al., 2008), *NANOG* mRNA levels were similar in EXOSC3-depleted hESCs and control cells (Figs. S1 C and 6 B), suggesting the reduction in ZNF143 upon exosome depletion (Fig. 5 G) was insufficient to down-regulate *NANOG*.

We next determined if exosome-mediated degradation of *FOXH1* mRNA was important for restraining differentiation. Although *FOXH1* protein is present in hESCs, transcription of its target genes is suppressed by a protein complex that sequesters its SMAD2/3 DNA-binding partners (Beyer et al., 2013). Upon induction of differentiation by Nodal/Activin/TGF-β signaling, SMAD2/3 interacts with FOXH1 to induce transcription of genes involved in forming ME, the precursor to the mesoderm and endoderm. Target genes include *NODAL*, *LEFTY1*, *CER1*, and the ME marker *MIXL1* (Kim et al., 2011b; Beyer et al., 2013; Reid et al., 2016). As expected if the exosome modulates ME formation by degrading *FOXH1* mRNA, expression of each of these FOXH1 targets increased in exosome-depleted EBs (Figs. 2 C and 7 A). To determine if increased levels of FOXH1 are sufficient to activate transcription of mRNAs encoding ME markers, we established stable hESC lines overexpressing FOXH1 (Fig. 7, B and C). Consistent with the hypothesis that increased FOXH1 is sufficient to drive ME formation, *CER1*, *NODAL*, and *MIXL1* mRNA levels increased in three independent FOXH1-overexpressing clones (Fig. 7 C).

We also confirmed that the increase in *FOXH1* mRNA upon exosome depletion was due to reduced degradation. EXOSC3-depleted hESCs were incubated with the transcription inhibitor 5,6-dichlorobenzimidazone-1-β-D-ribofuranoside (DRB) and the decay rates of the pre-mRNA and mRNA measured. As expected, *FOXH1* pre-mRNA was stabilized in EXOSC3-depleted hESCs, as its half-life increased to 30.0 ± 4.3 min, compared with 20.8 ± 0.4 min in hESCs treated with control siRNAs (Fig. 7 D). *FOXH1* mRNA half-lives were not significantly different between EXOSC3-depleted and control hESCs during the 30-min DRB incubation, indicating that the exosome may primarily exert its effects by degrading the pre-mRNA (Fig. 7 D). Control RNAs behaved as expected, as exosome depletion increased the half-life of a 3′ extended snoRNA but did not affect the decay rate of *NANOG* pre-mRNA (Fig. 7 D).

To test if exosome regulation of *FOXH1* mRNA enhances ME formation, we depleted EXOSC3 and/or FOXH1 in hESCs using siRNAs and incubated the cells with activin A, which induces formation of ME, followed by formation of definitive endoderm (D'Amour et al., 2005). We chose activin A because differentiation markers are detected within hours (D'Amour et al., 2005), making this system less susceptible to indirect effects than EB formation. We confirmed that EXOSC3 depletion from hESCs was >70% effective (Fig. 8 A, compare lanes 2 and 4 with lanes 1 and 3). Although *FOXH1* protein was not significantly increased in EXOSC3-depleted hESCs (Fig. 8 A, lane 2), the protein increased 2.3-fold in EXOSC3-depleted cells after activin A addition (lane 6). Examination of FOXH1 targets revealed that *CER1*, *NODAL*, *LEFTY1*, and *MIXL1* mRNAs were detectable within 2 h of adding activin A (Fig. 8 B). Importantly, all these mRNAs were significantly elevated in

EXOSC3-depleted cells within 4 h (Fig. 8 B). The increased mRNA levels required FOXH1, as the effects were abolished in cells depleted of EXOSC3 and FOXH1 (Fig. 8 B). These results were specific to FOXH1 targets, as two nontarget mRNAs, encoding AFP, a marker of visceral endoderm, and GAPDH, were unaffected (Fig. 8 B). Thus, by degrading *FOXH1* mRNA, the exosome restrains ME formation.

A shRNA-resistant transgene rescues phenotypes detected upon exosome depletion

To confirm that the exosome inhibits hESC differentiation, we tested if an shRNA-resistant transgene would rescue the phenotypes detected upon exosome depletion. Using hESC lines that express doxycycline-inducible shRNAs against *EXOSC3* mRNA as the parent cells, we generated two clonal cell lines that also stably express shRNA-resistant *EXOSC3* mRNA. As *EXOSC3* mRNA increased two- to fourfold in the shRNA-resistant cells, but the protein remained at or below WT levels (Fig. S5, A and B), EXOSC3 may be unstable when not assembled with other subunits. Exosomes from cells expressing the shRNA-resistant mRNA were functional, as the elevated PROMPTs detected upon EXOSC3 depletion decreased in the presence of the transgene (Fig. S5 C). L1 RNAs, lncRNAs and 3′ extended snoRNAs were also reduced (Fig. S5, C and D). Since depletions of hESCs with siRNAs were slightly more effective than shRNAs, we depleted two hESC lines expressing the shRNA-resistant *EXOSC3* transgene with an siRNA identical in sequence to the mature siRNA produced by the shRNA. Using this approach, levels of PROMPTS, L1 RNAs, lncRNAs, and *FOXH1* mRNA were all reduced in cells expressing the transgene (Figs. 9 A and S5 E).

We also tested whether the shRNA-resistant *EXOSC3* mRNA would restore the role of the exosome in preventing mesendoderm differentiation. To this end, we allowed shEXOSC3-depleted hESCs and two cell lines expressing the shEXOSC3-resistant transgene to differentiate to EBs. As expected, after 5 d of differentiation, EXOSC3-depleted EBs had increased levels of mRNAs encoding FOXH1 targets (*MIXL1*, *NODAL*, *LEFTY1*, and *CER1*) and other mRNAs that are markers of endoderm (*GATA4* and *SOX17*) and mesoderm (*EOMES*; Fig. 9 B). As these mRNAs were present at reduced levels in EBs expressing the shRNA-resistant transgene, we conclude that the exosome curtails hESC differentiation.

Discussion

Although the roles of transcription factors in controlling hESC identity are well known, the ways in which posttranscriptional processes regulate hESC fate are far less understood. We demonstrated that the RNA exosome restrains the differentiation of hESCs into endoderm, mesoderm, and ectoderm. A crucial target is the mRNA encoding FOXH1, a transcription factor required for ME formation.

The exosome as a regulator of hESC differentiation

Our data support a model in which the exosome contributes to hESC pluripotency by degrading RNAs that encode key developmental regulators. ESCs are unique in that they must both self-renew indefinitely and remain poised to differentiate into
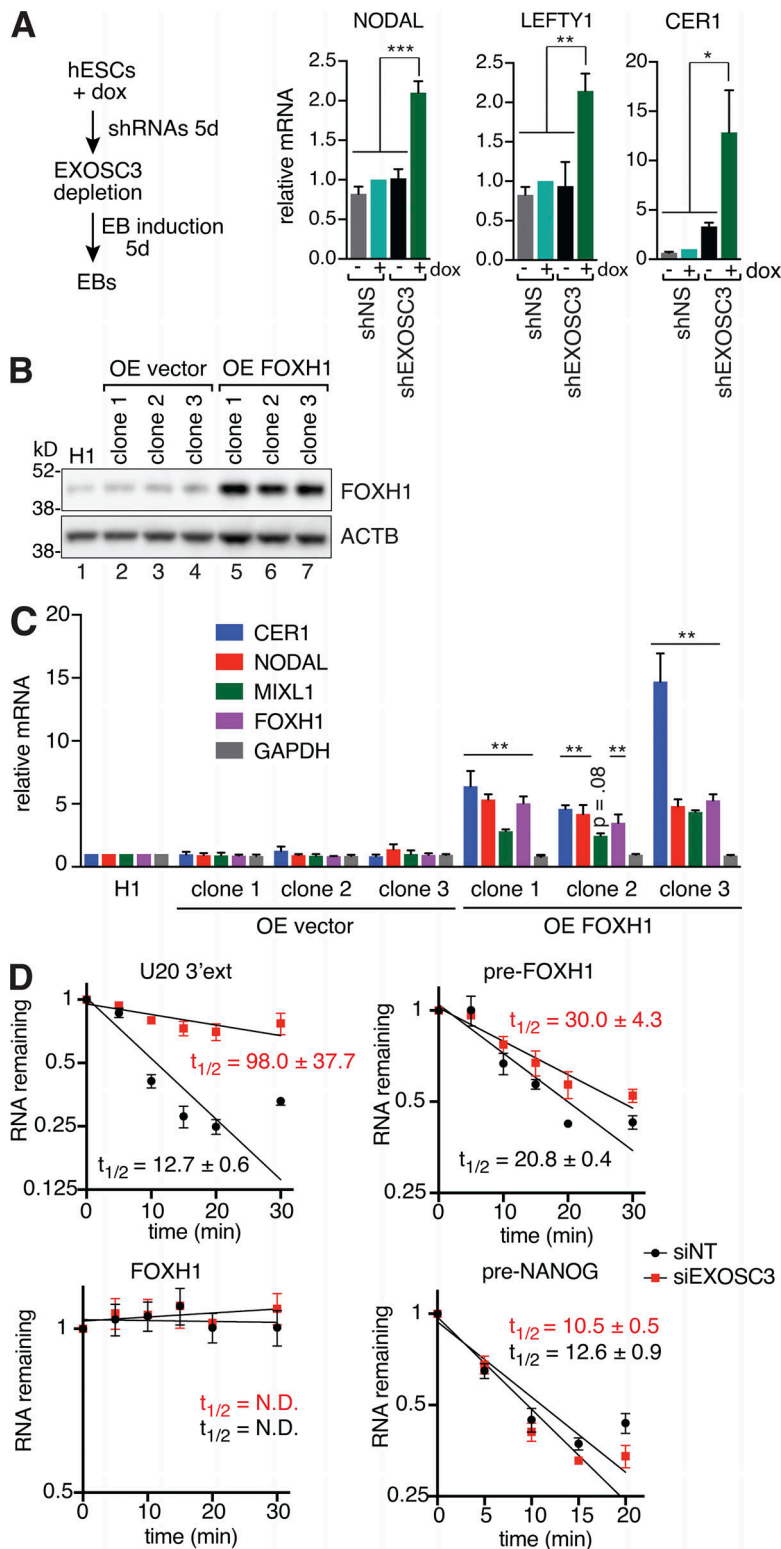
Figure 7. **Increased FOXH1 is sufficient to activate ME marker transcription. (A)** RT-qPCR analysis of *NODAL*, *LEFTY1* and *CER1* mRNAs in EXOSC3-depleted EBs. After culturing hESCs for 5 d, EBs were induced for another 5 d. Data are mean ± SEM (*n* = 3), relative to shNS cells in doxycycline and normalized to *ACTB*. **(B)** *FOXH1* protein was detected by immunoblotting in WT H1, control vector overexpressing (OE vector), and *FOXH1* mRNA-overexpressing (OE FOXH1) hESC clones. **(C)** RT-qPCR quantitation of *CER1*, *NODAL*, *MIXL1*, *FOXH1*, and control *GAPDH* mRNAs in WT H1 hESCs and H1 cells with empty vector (OE vector) or overexpressing FOXH1 (OE FOXH1). Data are mean ± SEM (*n* = 4). RNAs were normalized to *ACTB* relative to H1 hESCs. **(D)** After depletion with EXOSC3-2 or NT siRNAs, hESCs were incubated with 50 µM DRB. At the times shown, levels of the indicated RNAs were determined by RT-qPCR. To determine relative abundance and to calculate half-lives, mRNA levels were normalized to 18S rRNA, relative to t = 0 min. Data are mean ± SEM (*n* = 3). P values were calculated with one-way ANOVA. *, P < 0.05; **, P < 0.01; ***, P < 0.001.

all three germ layers. Although multiple mechanisms exist to repress transcription of lineage-specific regulators (Young, 2011), the exosome may function to degrade RNAs that escape other silencing pathways. Consistent with a role in maintaining pluripotency, the exosome is rapidly down-regulated when hESCs differentiate to EBs and up-regulated when fibroblasts are reprogrammed to iPSCs.

Although exosome-mediated degradation of *FOXH1* mRNA prevents ME induction, the full role of the exosome in restricting hESC differentiation undoubtedly involves other targets. Our finding that miR-205 increases in EXOSC3-depleted cells, coupled with a report that overexpressing this miRNA in mouse ESCs results in increased endoderm markers (Li et al., 2013), suggests that increased levels of this miRNA could
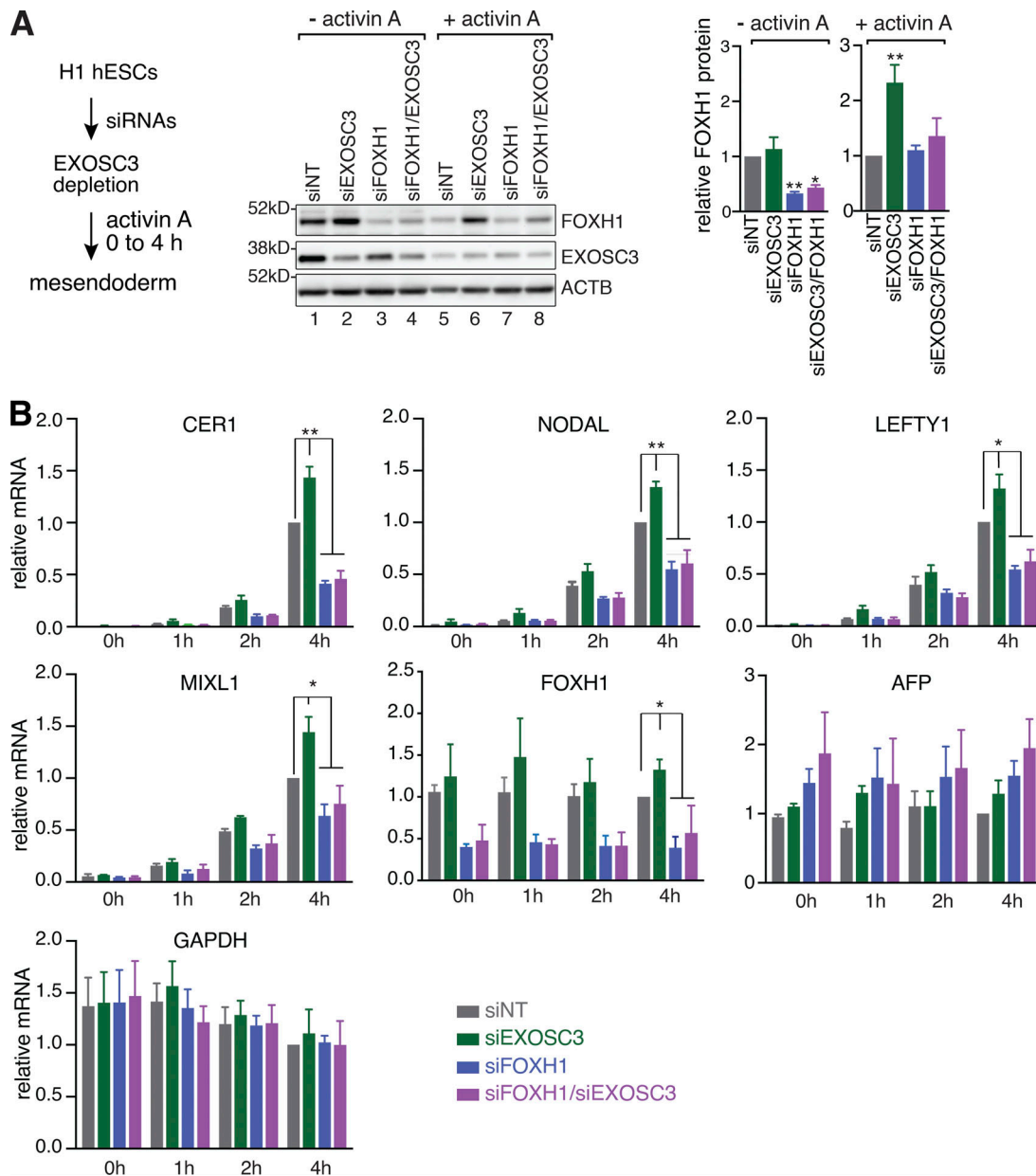
Figure 8. **Exosome degradation of *FOXH1* mRNA regulates ME formation.** **(A)** FOXH1 was quantitated by immunoblotting in siNT-, siEXOSC3-, and/or siFOXH1-treated cells with or without activin A treatment. Right: Quantitation of three biological replicates. Data are mean ± SEM (n = 3) normalized to ACTB and relative to siNT cells. **(B)** FOXH1 targets (*CER1*, *NODAL*, *LEFTY1*, and *MIXL1*) and control mRNAs (*AFP* and *GAPDH*) in cells treated with the indicated siRNAs and incubated with activin A were measured by RT-qPCR. *FOXH1* mRNA levels are also shown. Data are mean ± SEM (n = 4). RNAs were normalized to *ACTB* relative to siNT-treated cells after 4 h. P values were calculated with one-way ANOVA. *, P < 0.05; **, P < 0.01.

contribute to endoderm formation. Moreover, since ectoderm markers also increase in EXOSC3-depleted hESCs, other targets of the exosome must influence formation of this germ layer. Our description of the RNAs affected by exosome depletion may allow identification of these targets.

Our finding that multiple exosome subunits are rapidly down-regulated during differentiation, while mRNAs that encode the subunits are unchanged, implies that down-regulation occurs at the translational and/or posttranslational level. Notably, siRNA-mediated depletion of any of three tested core subunits (EXOSC3, EXOSC4, and EXOSC5)

reduces levels of the other two subunits as well as two of the three catalytic subunits (Kammler et al., 2008; Tomecki et al., 2010). Thus, inactivation of a single core subunit (through reduced translation, enhanced decay, or a posttranslational modification that impairs complex assembly) should be sufficient to rapidly down-regulate exosome activity. The ability of the exosome to undergo rapid inactivation may allow it to function as a developmental switch, allowing hESCs to quickly increase levels of mRNAs encoding key transcription factors such as FOXH1. At later times, transcriptional regulation may contribute to reducing exosome activity, since *EXOSC3* and
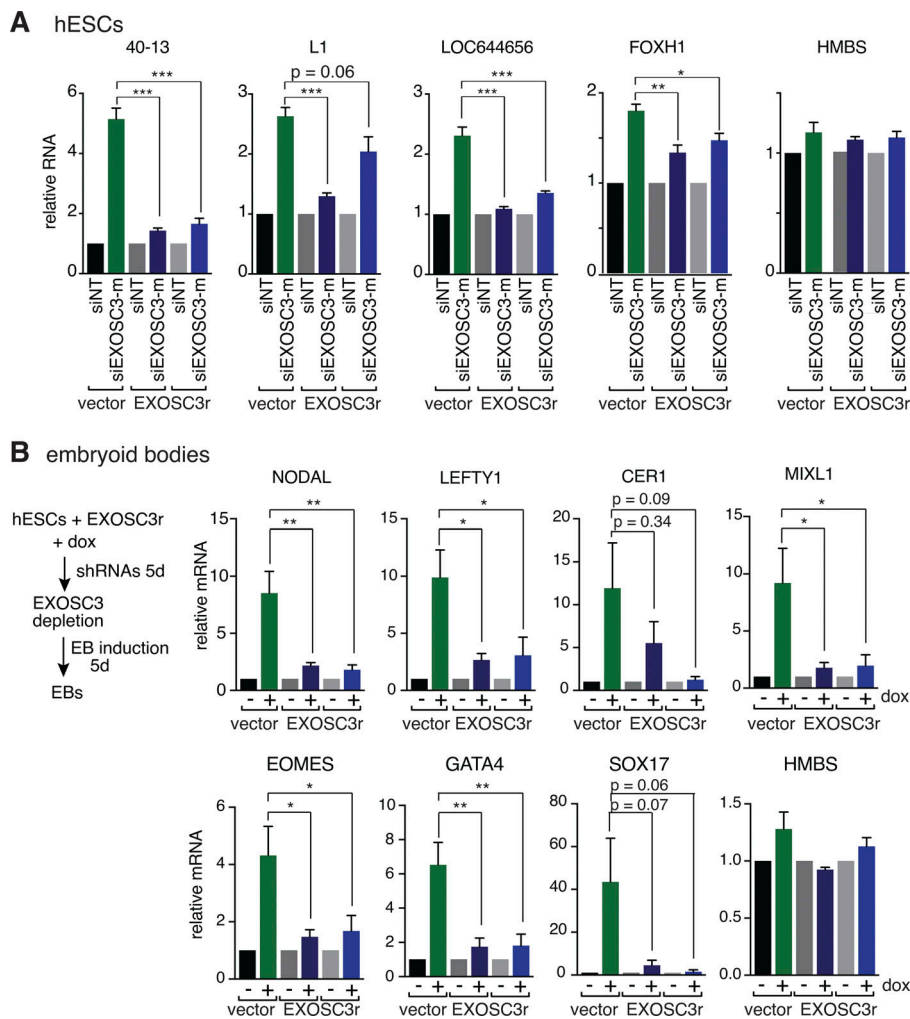
Figure 9. An shRNA-resistant transgene rescues phenotypes of exosome depletion. (A) shEXOSC3-expressing H1 hESCs carrying an empty vector or the shRNA-resistant EXOSC3 (EXOSC3r) transgene were treated with an siRNA that mimics mature shEXOSC3 RNA (siEXOSC3-m). RNAs were measured by RT-qPCR, normalized to *ACTB*, relative to the same cells treated with NT siRNA. Data are mean ± SEM (n = 4). **(B)** After 5 d of growth with or without doxycycline, H1 hESCs carrying empty vector or the shRNA-resistant *EXOSC3* transgene were differentiated into EBs for an additional 5 d. Levels of the indicated mRNAs were measured by RT-qPCR. Data are mean ± SEM (n = 4). RNAs were normalized to *ACTB* relative to the same cells without doxycycline. P values were calculated with one-way ANOVA. *, P < 0.05; **, P < 0.01; ***, P < 0.001.

EXOSC5 mRNAs were reported to decrease in EBs after 12 d (Fathi et al., 2009).

Our study, together with the finding that the NMD pathway is important for hESC differentiation (Lou et al., 2016), reveals that RNA decay pathways make key contributions to regulating hESC fate. In hESCs, NMD enhances mesoderm formation and limits definitive endoderm, although the mRNA targets responsible were not identified (Lou et al., 2016). Notably, human cells contain many pathways by which defective and potentially harmful mRNAs and ncRNAs can be targeted for decay (Schoenberg and Maquat, 2012; Belair et al., 2018). These pathways are often functionally overlapping, as it is often necessary to deplete multiple pathways to see significant accumulation of a specific target (Belair et al., 2018). Given that hESCs must both maintain the pluripotent state and retain the ability to rapidly differentiate in response to environmental signals, RNA surveillance pathways may function widely to degrade RNAs whose presence compromises hESC function. Although knowledge of how mammalian RNA decay pathways are regulated in response to environmental stimuli is limited, the ability of surveillance pathways to rapidly alter RNA levels may allow them to function as switches in a wide variety of developmental processes.

Additional roles for the exosome

Our data implicate the exosome in the defense against retrotransposition and revealed new ways in which the exosome modulates gene expression. Although the exosome had been implicated in pre-miRNA surveillance (Liu et al., 2014), we found that the EXOSC10-containing exosome affects miR-205 levels by reducing the pri-miRNA. The identification of 16S mt-rRNA as an exosome substrate opens the door to studying the poly(A) polymerases involved and raises questions as to the subcellular location where decay occurs. Although lncRNAs were known substrates (Flynn et al., 2011; Sigova et al., 2013), EXOSC3 depletion resulted in increased loc644656 lncRNA levels and resulted in a change in TSS usage for the adjacent *ZNF143*. Given the many antisense RNAs that are exosome targets, this mechanism of regulation could be widespread.

Materials and methods
Cell lines, cell culture, differentiation of hESCs, and decay assays
H1 and H9 hESCs were obtained from the Yale Stem Cell Core Facility. Cells were cultured on Matrigel (BD Biosciences)-coated plates under feeder-free conditions at 37°C in 5% CO_2, 5% O_2, and

90% humidity. Media consisted of DMEM/F12 (Invitrogen) supplemented with 1% MEM-nonessential amino acids (Invitrogen), 2 mM L-glutamine, 0.12 mM monothioglycerol, 0.5 mg/ml bovine serum albumin, 50 ng/ml basic fibroblast growth factor (Millipore), N2 supplements (1×), and B27 supplements (1×; Invitrogen). Media were changed every other day. Cells were passaged weekly by dissociating into small clumps with 1 mg/ml dispase (StemCell Technologies). Cells were used between passages 40 and 60 and tested regularly for mycoplasma. Alkaline phosphatase was detected using the Stemgent staining kit (Reprocell).

To establish hESCs stably expressing shRNAs, we used a modified piggyBac DNA transposon (Ding et al., 2005) in which the XbaI/PmeI fragment from pTRIPz (Dharmacon) containing the tetracycline-inducible promoter, the turboRFP reporter, the shRNA cassette, the human ubiquitin C promoter, the reverse tetracycline-transactivator 3, an internal ribosome entry site, a puromycin selection marker, and the woodchuck hepatitis posttranscriptional regulatory element was cloned between the left and right piggyBac repeat (PBL and PBR, respectively) transposon termini in *pBlueScript II SK+* (Stratagene). A rabbit β-globin poly(A) signal was added to ensure transcription termination (Ding et al., 2005). To create the EXOSC3 shRNA-expressing cassette, pTRIPz containing this shRNA (V3THS_306405; Dharmacon) was digested with NheI and XhoI and the shRNA-containing fragment was cloned into the same sites of the piggyBac construct. H1 ESCs were cotransfected with the shEXOSC3 piggyBac construct or a similar one expressing nonsilencing shRNA (gift of T. Xu, Yale University, New Haven, CT) together with the plasmid Act-PBase (Ding et al., 2005), which contains piggyBac transposase under control of the *ACTB* promoter. After 72 h, stable lines were selected in media containing 0.5 µg/ml puromycin. After 7 d selection, clonal lines were cultured in 0.8 µg/ml puromycin. For each cell line, shRNA transcription was induced with 2 µg/ml doxycycline and TurboRFP expression monitored by epifluorescence.

To stably overexpress FOXH1 in hESCs, *FOXH1* cDNA was amplified by RT-PCR from H1 ESC RNA using the Superscript III First Strand Synthesis System (Thermo Fisher) and the oligonucleotides listed in Table S2, digested with MluI, and cloned into a piggyBac transposon-based vector containing an *ACTB* promoter and a blasticidin S resistance cassette (Gayle et al., 2015; gift of T. Xu). H1 ESCs were cotransfected with either the *FOXH1* or empty piggyBac together with the plasmid Act-PBase using the P4 Primary Cell 4D-Nucleofector X Kit (Program CA137; Lonza). After 72 h, stable cell lines were selected in media containing 2 µg/ml Blasticidin. After 7 d, single colonies were isolated and analyzed.

To express the shEXOSC3 RNA-resistant transgene, *EXOSC3* cDNA was amplified from the plasmid pCMV6-EXOSC3 (RC200035; ORIGENE) with oligonucleotides EXOSC3-MluIF and EXOSC3-MluIR (Table S2), digested with MluI, and cloned into the piggyBac vector used to overexpress FOXH1. Silent mutations were introduced using the Q5 site-directed mutagenesis kit (New England Biolabs) using oligonucleotides EXOSC3-mut-F and EXOSC3-mut-R (Table S2). H1

ESCs were cotransfected with the shRNA-resistant *EXOSC3* in the piggyBac vector or the empty vector together with the plasmid Act-PBase using the P4 Primary Cell 4D-Nucleofector X Kit (Program CA137). After 72 h, stable cell lines were selected in media containing 2 µg/ml Blasticidin. After 7 d, single colonies were isolated and analyzed.

To produce EBs, hESCs were dissociated into clumps with 1 mg/ml dispase (StemCell Technologies) and cultured in DMEM/F12 media supplemented with 20% KnockOut Serum Replacement (Life Technologies), 2 mM L-glutamine, 0.1 mM MEM-nonessential amino acids, and 0.1 mM β-mercaptoethanol at 37°C in 5% CO_2, 21% O_2, and 90% humidity. Media were changed every other day. To form endoderm, cells were incubated with 100 ng/ml Activin A (Peprotech) in RPMI-1640 medium containing 0.2% FBS, 2 mM L-glutamine, and 0.1 mM MEM-nonessential amino acids at 37°C in 5% CO_2, 21% O_2, and 90% humidity.

To derive iPSCs, primary fibroblast cell lines were purchased from the Coriell Cell Repository and cultured in DMEM supplemented with 15% fetal bovine serum, 1 mM L-glutamine, 1% nonessential amino acids, and penicillin/streptomycin. To drive reprogramming to iPSCs, the cells were transduced with four retroviral reprogramming factors (*OCT4*, *SOX2*, *KLF4*, and *MYC*; Park et al., 2008; Kim et al., 2011a). The iPSCs were shown to have all features of pluripotent hESCs, including the ability to differentiate into all three germ layers. The iPSCs were maintained on Matrigel in mTeSR1 medium (StemCell Technologies). To monitor decay, hESCs were incubated with 50 µM DRB (Sigma) dissolved in DMSO. At the indicated times, TRIzol reagent (Thermo Fisher) was added to the culture dish and the RNA was extracted.

Transfections

Cells were transfected with siRNAs and plasmids as described previously (Ma et al., 2010). Briefly, after incubating for 1 h in media supplemented with 10 µM ROCK inhibitor Y-27632 (Selleckchem), hESC colonies were dissociated into single cells with Accutase (StemCell Technologies) and cells were harvested by centrifugation. After resuspending 2×10^6 cells in 200 µl siRNA (10 nM)/lipid mix and incubating 10–15 min at room temperature, 3 ml of prewarmed media containing 10 µM ROCK inhibitor Y-27632 was added, and the cells were transferred into a 60-mm Matrigel-coated dish and incubated overnight at 37°C in 5% CO_2, 5% O_2, and 90% humidity. Media were replaced the next day. For siRNAs, the first transfection was performed in duplicate, and the two sets of transfected cells were pooled for a second transfection after 48 h. Cells were harvested 72 h after the second transfection. A list of siRNAs is in Table S2. For plasmids, a single round of transfection was performed using 1.5 µg DNA.

Cell cycle measurements and cell viability assays

After incubating hESCs in fresh media containing 10 µM BrdU for 25 min, hESC colonies were dissociated into single cells with Accutase and fixed in 70% ethanol at 4°C overnight. Fixed cells were pelleted and incubated in 1 ml of 2 N HCl and 0.5% Triton X-100 for 30 min. After pelleting, cells were resuspended in

Belair et al.
The exosome regulates hESC differentiation

Journal of Cell Biology
2577
https://doi.org/10.1083/jcb.201811148

0.1 M $Na_2B_4O_7$, pH 8.5, pelleted, and resuspended in 75 µl of a mixture of 65 µl PBS, 0.5% Tween 20, 1% BSA, and 10 µl FITC-conjugated mouse anti-BrdU antibodies (clone 3D4; BD Biosciences) and incubated overnight at 4°C. Cell pellets were collected and resuspended in 500 µl PBS supplemented with 1 µg/ml DAPI for ≥30 min. Afterward, fluorescence was analyzed on a LSRII flow cytometer at the Yale FACS facility. To examine viability, hESC colonies were dissociated into single cells with Accutase, mixed with 1 vol Trypan Blue 0.4% Solution (Gibco), and counted with a hematocytometer.

RNA isolation, Northern blotting, and RT-qPCR

RNA was extracted with TRIzol reagent. For Northern blots, RNA was fractionated in 7% polyacrylamide-7 M urea gels and transferred to Hybond-N (GE Healthcare) in 0.5× TBE at 150 mA for 16 h. Membranes were hybridized at 42°C in 180 mM Na_2HPO_4, 80 mM NaH_2PO_4, 7% SDS, and 1 mM EDTA with 5′-^{32}P-labeled oligonucleotides. Blots were analyzed using a phosphorimager (Typhoon FLA 7000; GE Healthcare). For RT-qPCR, cDNA was synthesized with the Superscript III First-strand cDNA synthesis system (Thermo Fisher) and subjected to quantitative PCR with iTaq Universal SYBR Green Supermix (BioRad). To measure poly(A)-tailed RNAs, cDNA was made using Oligo(dT)$_{12-18}$ and Superscript III Reverse transcription (Invitrogen). Probes and primers are listed in Table S2.

Immunoblotting

After resuspending cells in lysis buffer (60 mM Tris-HCl, pH 7.5, 10% glycerol, and 2% SDS) with 1 mM PMSF and 1× protease inhibitor cocktail (Roche Diagnostics), incubating for 10 min at 4°C, and passing 10–15 times through a 27-gauge needle, lysates were cleared by sedimenting at 20,000 ×*g* for 15 min at 4°C. After SDS-PAGE, proteins were transferred to Immobilon-P (Millipore). Antibodies are listed in Table S2.

HITS-CLIP, PAR-iCLIP, and RNA sequencing (RNA-seq)

HITS-CLIP was performed largely as described previously (Darnell, 2012). Briefly, after irradiating H1 cells with 600 mJ/cm², cells were harvested in cold 1× Dulbecco's PBS (Gibco) and sedimented at 300 ×*g*. After resuspending pellets in 400 µl lysis buffer (1× PBS, 0.1% SDS, 0.5% deoxycholate, and 0.5% NP-40) with EDTA-free protease inhibitors (Roche) and 1 mM PMSF, incubating 10 min on ice, adding 50 U DNase I (Roche), and incubating at 37°C for 10 min, EDTA was added to 1 mM final concentration and lysates were cleared by sedimenting twice at 20,000 ×*g* for 10 min at 4°C. Antibodies (10 µg) were conjugated with 50 µl Dynabeads Protein G (Life Technologies) for 1 h at 4°C in 400 µl lysis buffer. After preclearing for 10 min at 4°C with 50 µl Dynabeads Protein G, lysates were incubated with antibody-conjugated beads for 1 h at 4°C. Beads were washed three times with PXL + E (5× PBS, 0.1% SDS, 0.5% deoxycholate, 0.5% NP-40, and 1 mM EDTA), three times with H-RIPA (50 mM Tris-HCl pH 7.5, 400 mM NaCl, 1% NP-40, 1% deoxycholate, 0.1% SDS, 1 mM EDTA, and 0.2 M urea), and three times with PNK buffer (50 mM Tris-HCl, pH 7.5, 10 mM $MgCl_2$, and 0.5% NP-40). Beads were resuspended in 500 µl MNase buffer (50 mM Tris-HCl, pH 8, and 5 mM $CaCl_2$) with 20 U or 0.2 U micrococcal

nuclease and incubated 1 min at 37°C, followed by 10 min on ice. After washing twice in PNK + EGTA (50 mM Tris-HCl, pH 7.5, 20 mM EGTA, and 0.5% NP-40) and twice in PNK, beads were treated with 2 U rApid alkaline phosphatase (Roche) for 10 min at 37°C and washed twice each with PNK + EGTA and PNK buffers. Next, 3′ linkers were ligated to the RNA overnight at 4°C in 40 µl containing 80 pmol RL3 RNA linker, 4 µg BSA, 1 mM ATP, 40 U RNaseOUT (Life Technologies), and 10 U T4 RNA ligase. After two washes in PXL and PNK buffers, RNAs on beads were 5′-labeled with [γ-^{32}P]ATP and 20 U T4 polynucleotide kinase in PNK buffer for 30 min at 37°C, 5 µl ATP (1 mM) was added, and the reaction was incubated an additional 10 min at 37°C. After two washes in H-RIPA and PNK buffers, RNPs were eluted by heating beads at 95°C twice for 5 min each in elution buffer (2× NuPage LDS sample buffer [Life Technologies] in PNK + EGTA). Complexes were resolved in a NuPage Novex 10% Bis-Tris gel (Life Technologies) and transferred to BA-85 nitrocellulose (Sigma-Aldrich). Bands corresponding to proteins cross-linked to ~50 nt RNAs were excised and digested with 4 mg/ml Proteinase K in 200 µl PK buffer (100 mM Tris-HCl, pH 7.5, 50 mM NaCl, and 10 mM EDTA) for 20 min at 37°C. After adding 200 µl of Proteinase K/7M urea in PK buffer, incubating for another 20 min at 37°C, an equal volume of phenol/chloroform/isoamyl alcohol (25:24:1) was added and incubated for 20 min at 37°C. After removing the aqueous phase, RNA was precipitated with 1 ml of 1:1 ethanol/isopropanol. Afterward, 5′ linkers were ligated for 1 h at 16°C in 10 µl containing 20 pmol RL5 RNA linker, 1 µg BSA, 1 mM ATP, and 1 U T4 RNA ligase. After adding 50 U RQ1 DNase I (Roche) and incubating for 20 min, RNA was isolated by extracting with phenol/chloroform/isoamyl alcohol (25:24:1) and precipitated with 2.5 vol of 1:1 ethanol/isopropanol. Next, RNA was resuspended in 10 µl H_2O containing 10 pmol primer DP3 and 10 µmol dNTPs, heated at 65°C for 5 min, and reverse transcribed with 200 U Superscript III (Life Technologies) for 45 min at 50°C and 55°C for 15 min. After heating at 90°C for 5 min, PCR was performed using AccuPrime Pfx SuperMix (Life Technologies), 15 pmol each of primers DP3 and DP5, and 2 µl cDNA. After gel-purifying ~110–150 bp DNAs and multiplexing by performing PCR with AccuPrime Pfx SuperMix, 10 pmol DSPF5 primer, 10 pmol 3′ index primer, and 1 µl DNAs, DNAs were gel purified and subjected to 75-bp single-end Illumina HiSeq 2000 sequencing at the Yale Center for Genome analysis. Antibodies, RNA linkers, and PCR primers are listed in Table S2.

PAR-iCLIP was performed as described previously (Huppertz et al., 2014). Briefly, after incubating hESCs with 100 µM 4-thiouridine for 7 h, cells were irradiated with 800 mJ/cm² UV light (365 nm). After sonication in 50 mM Tris-HCl, pH 7.4, 100 mM NaCl, 0.1% SDS, 0.5% deoxycholate, 1% NP-40, and 1 mM EDTA, lysates were incubated with 20 U Turbo DNase (Invitrogen) and 100 U RNase I (Invitrogen) at 37°C for 10 min, followed by immunoprecipitation with anti-EXOSC4 antibody (A303-775A; Bethyl) conjugated to Dynabeads Protein G (Invitrogen). Beads were washed with high-salt wash buffer (50 mM Tris-HCl, pH 7.4, 1 M NaCl, 0.1% SDS, 0.5% deoxycholate, 1% NP-40, and 1 mM EDTA) and incubated with T4 PNK (NEB), followed by 3′ linker ligation. After labeling RNA with ^{32}P, the protein–RNA

complex was fractionated in a 10% NuPAGE Bis-Tris gel (Invitrogen) and transferred to nitrocellulose. After autoradiography, protein–RNA complexes were excised and RNAs were eluted from the membrane. After reverse transcription using Superscript III (Invitrogen) and primers containing 9 nt barcodes (4 nt for sample discrimination and 5 nt to identify PCR duplicates), cDNAs were gel purified, circularized with Circligase II (Epicentre), and cut using BamHI and a BamHI site–containing complementary oligonucleotide. Linearized cDNA was amplified using Phusion High-Fidelity PCR Master Mix (NEB) and sequenced on Illumina NEXTSeq.

For RNA-seq, RNA integrity was verified on a 2100 Bioanalyzer (Agilent Technologies), ERCC ExFold RNA Spike-In mix (Life Technologies) was added, and rRNAs were removed using Ribo-Zero (Epicentre). Libraries were prepared using ScriptSeq v2 RNA-seq Library Preparation kits (Epicentre) and multiplexed with ScriptSeq Index PCR primers (Epicentre). Libraries were submitted for 50- or 75-bp single-end Illumina HiSeq 2000 sequencing at the Yale Center for Genome Analysis and the Yale Stem Cell Genomics Core Facility. 25–50 million reads were obtained per library.

Immunoprecipitations from UV-cross-linked cells

Cells were irradiated and immunoprecipitated as described for HITS-CLIP, except that 1 U/μl RNaseOUT recombinant ribonuclease inhibitor (Thermo Fisher) was added to the lysis buffer, and RNase was omitted. After incubating 1 h at 4°C with anti-EXOSC4 antibodies or control IgG, beads were washed five times with 5× PXL containing 1 mM EDTA, H-RIPA, and PNK+ buffers. RNAs were eluted by incubating the beads for 20 min at 37°C in PK buffer containing 4 mg/ml proteinase K and adding 200 μl 7 M urea PK buffer, followed by a second incubation for 20 min at 37°C, phenol/chloroform extraction, and ethanol precipitation. 5% of the lysate was subjected directly to phenol/chloroform extraction and ethanol precipitation. Following DNase I treatment, cDNA was prepared using SuperScript III First-Strand Synthesis System (Thermo Fisher) and subjected to quantitative PCR with iTaq Universal SYBR Green Supermix (BioRad). Cq (quantitation cycle) values were adjusted to the total quantity of RNAs obtained for each sample (input, IgG, and EXOSC4), and the fold enrichment over IgG control was calculated using the ΔCq method. A Cq value of 40 was used when no signal was detected during quantitative PCR.

Bioinformatics

After RNA-seq, reads were processed using the FASTX-Toolkit to remove low-quality, short (<16 nt) reads and adapters. After removing reads mapping to rRNAs, >98% of reads aligned to the human genome (hg19/GRCh37) using TopHat (Kim et al., 2013). Differential expression analyses were performed using Cufflinks (Trapnell et al., 2010). Genome coverage was done using Bedtools (genomeCoverageBed; Quinlan and Hall, 2010). As the number of reads that mapped to the genome differed between samples, a scale was applied for each library. This scale corresponds to the ratio between the total number of reads mapped to the genome for each library and the lowest number obtained from each set of libraries (5 or 7 d). RNA-seq reads for repeat

elements were quantified using Salmon (Patro et al., 2017). Consensus sequences of repeat elements in the human genome were downloaded from the Repbase database (Bao et al., 2015) and used as reference transcripts for counting.

Gene expression levels were estimated as reads per kilo million by Cufflinks (v1.2.1) using RefSeq genes as the reference (Trapnell et al., 2010). GO analysis was then performed on genes whose difference in expression between doxycycline- treated and untreated cells was >1.5 fold, with GO stats (v2.24.0) library in Bioconductor (Falcon and Gentleman, 2007). The P value for each GO term was adjusted by the Benjamini–Hochberg method with the p.adjust function in R to obtain the false discovery rate. For the heat map, genes were selected from the list of differentially expressed genes which had GO terms related to cell development (e.g., muscle organ development).

HITS-CLIP and PAR-iCLIP reads were preprocessed using Cutadapt (Martin, 2011) and FASTX-Toolkit to remove adaptors and low-quality reads, collapsed to remove duplicates, and split by barcodes. Reads were then aligned to the hg19 genome using Novoalign. Since CLIP experiments can generate multiple mismatches and deletions within reads, the mapping stringency was lowered (-t 15,3 -l 20 -x 4 -g 20). Reads that could be mapped to multiple loci in the genome were allowed to map once to a randomly chosen locus with the best mapping score. For the coverage pie charts, reads were counted for each category using Bedtools (Quinlan and Hall, 2010) based on annotations from the University of California Santa Cruz genome browser. For L1Hs, libraries were mapped against a consensus sequence from Repbase (Bao et al., 2015). Read clusters for PAR-iCLIP were analyzed using Paralyzer v1.5 (Corcoran et al., 2011).

Statistical analyses

Data are shown as means ± SEMs, with the number of replicates in parentheses. Significances of differences between samples were evaluated using one-way ANOVA or two-tailed unpaired t test. P values <0.05 were considered to represent significant differences. P values are represented as *, **, and ***, corresponding to P ≤ 0.05, P ≤ 0.01, and P ≤ 0.001, respectively.

Accession numbers

The data associated with this manuscript have been deposited to the Gene Expression Omnibus and are available under accession no. GSE132469.

Online supplemental material

Fig. S1 shows the effects of EXOSC3 depletion on proliferation and pluripotency markers. Fig. S2 shows additional evidence that mRNAs encoding differentiation markers increase in EXOSC3-depleted hESCs and EBs, and that exosome subunits are down-regulated when hESCs are differentiated to form EBs. Fig. S3 shows the autoradiograms from the HITS-CLIP and PAR-iCLIP experiments and the effects of exosome depletion on snoRNA, snRNA, and telomerase RNA targets. Fig. S4 provides additional data that *FOXH1*, *CDKN1A*, and *ZCCHC8* mRNAs are exosome targets. Fig. S5 shows the characterization of hESCs expressing an shRNA-resistant EXOSC3 transgene. Table S1 reports the RNA-seq data for mRNAs and ncRNAs, HITS-CLIP

and PAR-iCLIP tag counts, and PAR-iCLIP clusters. Table S2 lists the primers, oligonucleotide probes, antibodies, and siRNAs used in this study.

Acknowledgments

References

Bailey, S.D., X. Zhang, K. Desai, M. Aid, O. Corradin, R. Cowper-Sal Lari, B. Akhtar-Zaidi, P.C. Scacheri, B. Haibe-Kains, and M. Lupien. 2015. ZNF143 provides sequence specificity to secure chromatin interactions at gene promoters. *Nat. Commun.* 2:6186. https://doi.org/10.1038/ncomms7186

Bao, W., K.K. Kojima, and O. Kohany. 2015. Repbase Update, a database of repetitive elements in eukaryotic genomes. *Mob. DNA.* 6:11. https://doi.org/10.1186/s13100-015-0041-9

Beck, C.R., J.L. Garcia-Perez, R.M. Badge, and J.V. Moran. 2011. LINE-1 elements in structural variation and disease. *Annu. Rev. Genomics Hum. Genet.* 12:187–215. https://doi.org/10.1146/annurev-genom-082509-141802

Belair, C., S. Sim, and S.L. Wolin. 2018. Noncoding RNA Surveillance: The Ends Justify the Means. *Chem. Rev.* 118:4422–4447. https://doi.org/10.1021/acs.chemrev.7b00462

Bernstein, B.E., T.S. Mikkelsen, X. Xie, M. Kamal, D.J. Huebert, J. Cuff, B. Fry, A. Meissner, M. Wernig, K. Plath, et al. 2006. A bivalent chromatin structure marks key developmental genes in embryonic stem cells. *Cell.* 125:315–326. https://doi.org/10.1016/j.cell.2006.02.041

Beyer, T.A., A. Weiss, Y. Khomchuk, K. Huang, A.A. Ogunjimi, X. Varelas, and J.L. Wrana. 2013. Switch enhancers interpret TGF-β and Hippo signaling to control cell fate in human embryonic stem cells. *Cell Reports.* 5:1611–1624. https://doi.org/10.1016/j.celrep.2013.11.021

Bhattaram, P., A. Penzo-Méndez, E. Sock, C. Colmenares, K.J. Kaneko, A. Vassilev, M.L. Depamphilis, M. Wegner, and V. Lefebvre. 2010. Organogenesis relies on SoxC transcription factors for the survival of neural and mesenchymal progenitors. *Nat. Commun.* 1:9. https://doi.org/10.1038/ncomms1008

Brickman, J.M., and P. Serup. 2017. Properties of embryoid bodies. *Wiley Interdiscip. Rev. Dev. Biol.* 6:e259. https://doi.org/10.1002/wdev.259

Castello, A., B. Fischer, K. Eichelbaum, R. Horos, B.M. Beckmann, C. Strein, N.E. Davey, D.T. Humphreys, T. Preiss, L.M. Steinmetz, et al. 2012. Insights into RNA biology from an atlas of mammalian mRNA-binding proteins. *Cell.* 149:1393–1406. https://doi.org/10.1016/j.cell.2012.04.031

Chen, X., F. Fang, Y.C. Liou, and H.H. Ng. 2008. Zfp143 regulates Nanog through modulation of Oct4 binding. *Stem Cells.* 26:2759–2767. https://doi.org/10.1634/stemcells.2008-0398

Chia, N.Y., Y.S. Chan, B. Feng, X. Lu, Y.L. Orlov, D. Moreau, P. Kumar, L. Yang, J. Jiang, M.S. Lau, et al. 2010. A genome-wide RNAi screen reveals determinants of human embryonic stem cell identity. *Nature.* 468:316–320. https://doi.org/10.1038/nature09531

Corcoran, D.L., S. Georgiev, N. Mukherjee, E. Gottwein, R.L. Skalsky, J.D. Keene, and U. Ohler. 2011. PARalyzer: definition of RNA binding sites from PAR-CLIP short-read sequence data. *Genome Biol.* 12:R79. https://doi.org/10.1186/gb-2011-12-8-r79

D'Amour, K.A., A.D. Agulnick, S. Eliazer, O.G. Kelly, E. Kroon, and E.E. Baetge. 2005. Efficient differentiation of human embryonic stem cells to definitive endoderm. *Nat. Biotechnol.* 23:1534–1541. https://doi.org/10.1038/nbt1163

Darnell, R. 2012. CLIP (cross-linking and immunoprecipitation) identification of RNAs bound by a specific protein. *Cold Spring Harb. Protoc.* 2012:1146–1160. https://doi.org/10.1101/pdb.prot072132

De Los Angeles, A., F. Ferrari, R. Xi, Y. Fujiwara, N. Benvenisty, H. Deng, K. Hochedlinger, R. Jaenisch, S. Lee, H.G. Leitch, et al. 2015. Hallmarks of pluripotency. *Nature.* 525:469–478. https://doi.org/10.1038/nature15515

Ding, S., X. Wu, G. Li, M. Han, Y. Zhuang, and T. Xu. 2005. Efficient transposition of the piggyBac (PB) transposon in mammalian cells and mice. *Cell.* 122:473–483. https://doi.org/10.1016/j.cell.2005.07.013

Dolezalova, D., M. Mraz, T. Barta, K. Plevova, V. Vinarsky, Z. Holubcova, J. Jaros, P. Dvorak, S. Pospisilova, and A. Hampl. 2012. MicroRNAs regulate p21(Waf1/Cip1) protein expression and the DNA damage response in human embryonic stem cells. *Stem Cells.* 30:1362–1372. https://doi.org/10.1002/stem.1108

Duperret, E.K., A. Dahal, and T.W. Ridky. 2015. Focal-adhesion-independent integrin-αv regulation of FAK and c-Myc is necessary for 3D skin formation and tumor invasion. *J. Cell Sci.* 128:3997–4013. https://doi.org/10.1242/jcs.175539

Efroni, S., R. Duttagupta, J. Cheng, H. Dehghani, D.J. Hoeppner, C. Dash, D.P. Bazett-Jones, S. Le Grice, R.D. McKay, K.H. Buetow, et al. 2008. Global transcription in pluripotent embryonic stem cells. *Cell Stem Cell.* 2:437–447. https://doi.org/10.1016/j.stem.2008.03.021

Falcon, S., and R. Gentleman. 2007. Using GOstats to test gene lists for GO term association. *Bioinformatics.* 23:257–258. https://doi.org/10.1093/bioinformatics/btl567

Fathi, A., M. Pakzad, A. Taei, T.C. Brink, L. Pirhaji, G. Ruiz, M. Sharif Tabe Bordbar, H. Gourabi, J. Adjaye, H. Baharvand, and G.H. Salekdeh. 2009. Comparative proteome and transcriptome analyses of embryonic stem cells during embryoid body-based differentiation. *Proteomics.* 9:4859–4870. https://doi.org/10.1002/pmic.200900003

Flynn, R.A., A.E. Almada, J.R. Zamudio, and P.A. Sharp. 2011. Antisense RNA polymerase II divergent transcripts are P-TEFb dependent and substrates for the RNA exosome. *Proc. Natl. Acad. Sci. USA.* 108:10460–10465. https://doi.org/10.1073/pnas.1106630108

Fort, A., K. Hashimoto, D. Yamada, M. Salimullah, C.A. Keya, A. Saxena, A. Bonetti, I. Voineagu, N. Bertin, A. Kratz, et al. FANTOM Consortium. 2014. Deep transcriptome profiling of mammalian stem cells supports a regulatory role for retrotransposons in pluripotency maintenance. *Nat. Genet.* 46:558–566. https://doi.org/10.1038/ng.2965

Garcia-Perez, J.L., M.C. Marchetto, A.R. Muotri, N.G. Coufal, F.H. Gage, K.S. O'Shea, and J.V. Moran. 2007. LINE-1 retrotransposition in human embryonic stem cells. *Hum. Mol. Genet.* 16:1569–1577. https://doi.org/10.1093/hmg/ddm105

Gaspar-Maia, A., A. Alajem, E. Meshorer, and M. Ramalho-Santos. 2011. Open chromatin in pluripotency and reprogramming. *Nat. Rev. Mol. Cell Biol.* 12:36–47. https://doi.org/10.1038/nrm3036

Gayle, S., Y. Pan, S. Landrette, and T. Xu. 2015. piggyBac insertional mutagenesis screen identifies a role for nuclear RHOA in human ES cell differentiation. *Stem Cell Reports.* 4:926–938. https://doi.org/10.1016/j.stemcr.2015.03.001

Gregory, P.A., A.G. Bert, E.L. Paterson, S.C. Barry, A. Tsykin, G. Farshid, M.A. Vadas, Y. Khew-Goodall, and G.J. Goodall. 2008. The miR-200 family and miR-205 regulate epithelial to mesenchymal transition by targeting ZEB1 and SIP1. *Nat. Cell Biol.* 10:593–601. https://doi.org/10.1038/ncb1722

Hafner, M., M. Landthaler, L. Burger, M. Khorshid, J. Hausser, P. Berninger, A. Rothballer, M. Ascano Jr., A.C. Jungkamp, M. Munschauer, et al. 2010. Transcriptome-wide identification of RNA-binding protein and microRNA target sites by PAR-CLIP. *Cell.* 141:129–141. https://doi.org/10.1016/j.cell.2010.03.009

Hoodless, P.A., M. Pye, C. Chazaud, E. Labbé, L. Attisano, J. Rossant, and J.L. Wrana. 2001. FoxH1 (Fast) functions to specify the anterior primitive streak in the mouse. *Genes Dev.* 15:1257–1271. https://doi.org/10.1101/gad.881501

Huppertz, I., J. Attig, A. D'Ambrogio, L.E. Easton, C.R. Sibley, Y. Sugimoto, M. Tajnik, J. König, and J. Ule. 2014. iCLIP: protein-RNA interactions at nucleotide resolution. *Methods.* 65:274–287. https://doi.org/10.1016/j.ymeth.2013.10.011

Kammler, S., S. Lykke-Andersen, and T.H. Jensen. 2008. The RNA exosome component hRrp6 is a target for 5-fluorouracil in human cells. *Mol. Cancer Res.* 6:990–995. https://doi.org/10.1158/1541-7786.MCR-07-2217

Kanellopoulou, C., S.A. Muljo, A.L. Kung, S. Ganesan, R. Drapkin, T. Jenuwein, D.M. Livingston, and K. Rajewsky. 2005. Dicer-deficient mouse embryonic stem cells are defective in differentiation and centromeric silencing. *Genes Dev.* 19:489–501. https://doi.org/10.1101/gad.1248505

Kim, D., G. Pertea, C. Trapnell, H. Pimentel, R. Kelley, and S.L. Salzberg. 2013. TopHat2: accurate alignment of transcriptomes in the presence of insertions, deletions and gene fusions. *Genome Biol.* 14:R36. https://doi.org/10.1186/gb-2013-14-4-r36

Kim, K.Y., E. Hysolli, and I.H. Park. 2011a. Neuronal maturation defect in induced pluripotent stem cells from patients with Rett syndrome. *Proc. Natl. Acad. Sci. USA.* 108:14169–14174. https://doi.org/10.1073/pnas.1018979108

Kim, S.W., S.J. Yoon, E. Chuong, C. Oyolu, A.E. Wills, R. Gupta, and J. Baker. 2011b. Chromatin and transcriptional signatures for Nodal signaling during endoderm formation in hESCs. *Dev. Biol.* 357:492–504. https://doi.org/10.1016/j.ydbio.2011.06.009

Labbé, E., C. Silvestri, P.A. Hoodless, J.L. Wrana, and L. Attisano. 1998. Smad2 and Smad3 positively and negatively regulate TGF beta-dependent transcription through the forkhead DNA-binding protein FAST2. *Mol. Cell.* 2:109–120. https://doi.org/10.1016/S1097-2765(00)80119-7

Li, C., D. Finkelstein, and C.J. Sherr. 2013. Arf tumor suppressor and miR-205 regulate cell adhesion and formation of extraembryonic endoderm from pluripotent stem cells. *Proc. Natl. Acad. Sci. USA.* 110:E1112–E1121. https://doi.org/10.1073/pnas.1302184110

Licatalosi, D.D., A. Mele, J.J. Fak, J. Ule, M. Kayikci, S.W. Chi, T.A. Clark, A.C. Schweitzer, J.E. Blume, X. Wang, et al. 2008. HITS-CLIP yields genome-wide insights into brain alternative RNA processing. *Nature.* 456:464–469. https://doi.org/10.1038/nature07488

Liu, X., Q. Zheng, N. Vrettos, M. Maragkakis, P. Alexiou, B.D. Gregory, and Z. Mourelatos. 2014. A MicroRNA precursor surveillance system in quality control of MicroRNA synthesis. *Mol. Cell.* 55:868–879. https://doi.org/10.1016/j.molcel.2014.07.017

Lou, C.H., J. Dumdie, A. Goetz, E.Y. Shum, D. Brafman, X. Liao, S. Mora-Castilla, M. Ramaiah, H. Cook-Andersen, L. Laurent, and M.F. Wilkinson. 2016. Nonsense-mediated RNA decay influences human embryonic stem cell fate. *Stem Cell Reports.* 6:844–857. https://doi.org/10.1016/j.stemcr.2016.05.008

Lubas, M., M.S. Christensen, M.S. Kristiansen, M. Domanski, L.G. Falkenby, S. Lykke-Andersen, J.S. Andersen, A. Dziembowski, and T.H. Jensen. 2011. Interaction profiling identifies the human nuclear exosome targeting complex. *Mol. Cell.* 43:624–637. https://doi.org/10.1016/j.molcel.2011.06.028

Lubas, M., P.R. Andersen, A. Schein, A. Dziembowski, G. Kudla, and T.H. Jensen. 2015. The human nuclear exosome targeting complex is loaded onto newly synthesized RNA to direct early ribonucleolysis. *Cell Reports.* 10:178–192. https://doi.org/10.1016/j.celrep.2014.12.026

Ma, Y., J. Jin, C. Dong, E.C. Cheng, H. Lin, Y. Huang, and C. Qiu. 2010. High-efficiency siRNA-based gene knockdown in human embryonic stem cells. *RNA.* 16:2564–2569. https://doi.org/10.1261/rna.2350710

Macias, S., R.A. Cordiner, P. Gautier, M. Plass, and J.F. Cáceres. 2015. DGCR8 acts as an adaptor for the exosome complex to degrade double-stranded structured RNAs. *Mol. Cell.* 60:873–885. https://doi.org/10.1016/j.molcel.2015.11.011

Martin, M. 2011. Cutadapt removes adapter sequences from high-throughput sequencing reads. *EMBnet.Journal.* 17:10–12.

McIver, S.C., Y.A. Kang, A.W. DeVilbiss, C.A. O'Driscoll, J.N. Ouellette, N.J. Pope, G. Camprecios, C.J. Chang, D. Yang, E.E. Bouhassira, et al. 2014. The exosome complex establishes a barricade to erythroid maturation. *Blood.* 124:2285–2297. https://doi.org/10.1182/blood-2014-04-571083

Mistry, D.S., Y. Chen, and G.L. Sen. 2012. Progenitor function in self-renewing human epidermis is maintained by the exosome. *Cell Stem Cell.* 11:127–135. https://doi.org/10.1016/j.stem.2012.04.022

Mitchell, P., E. Petfalski, A. Shevchenko, M. Mann, and D. Tollervey. 1997. The exosome: a conserved eukaryotic RNA processing complex containing multiple 3′-->5′ exoribonucleases. *Cell.* 91:457–466. https://doi.org/10.1016/S0092-8674(00)80432-8

Moore, M.J., C. Zhang, E.C. Gantman, A. Mele, J.C. Darnell, and R.B. Darnell. 2014. Mapping Argonaute and conventional RNA-binding protein interactions with RNA at single-nucleotide resolution using HITS-CLIP and CIMS analysis. *Nat. Protoc.* 9:263–293. https://doi.org/10.1038/nprot.2014.012

Morton, D.J., E.G. Kuiper, S.K. Jones, S.W. Leung, A.H. Corbett, and M.B. Fasken. 2018. The RNA exosome and RNA exosome-linked disease. *RNA.* 24:127–142. https://doi.org/10.1261/rna.064626.117

Ngondo, R.P., and P. Carbon. 2014. Transcription factor abundance controlled by an auto-regulatory mechanism involving a transcription start site switch. *Nucleic Acids Res.* 42:2171–2184. https://doi.org/10.1093/nar/gkt1136

Ngondo-Mbongo, R.P., E. Myslinski, J.C. Aster, and P. Carbon. 2013. Modulation of gene expression via overlapping binding sites exerted by ZNF143, Notch1 and THAP11. *Nucleic Acids Res.* 41:4000–4014. https://doi.org/10.1093/nar/gkt088

Nguyen, D., V. Grenier St-Sauveur, D. Bergeron, F. Dupuis-Sandoval, M.S. Scott, and F. Bachand. 2015. A Polyadenylation-Dependent 3′ End Maturation Pathway Is Required for the Synthesis of the Human Telomerase RNA. *Cell Reports.* 13:2244–2257. https://doi.org/10.1016/j.celrep.2015.11.003

Ogami, K., Y. Chen, and J.L. Manley. 2018. RNA surveillance by the nuclear RNA exosome: mechanisms and significance. *Noncoding RNA.* 4:4.

Park, I.H., R. Zhao, J.A. West, A. Yabuuchi, H. Huo, T.A. Ince, P.H. Lerou, M.W. Lensch, and G.Q. Daley. 2008. Reprogramming of human somatic cells to pluripotency with defined factors. *Nature.* 451:141–146. https://doi.org/10.1038/nature06534

Patro, R., G. Duggal, M.I. Love, R.A. Irizarry, and C. Kingsford. 2017. Salmon provides fast and bias-aware quantification of transcript expression. *Nat. Methods.* 14:417–419. https://doi.org/10.1038/nmeth.4197

Polo, J.M., E. Anderssen, R.M. Walsh, B.A. Schwarz, C.M. Nefzger, S.M. Lim, M. Borkent, E. Apostolou, S. Alaei, J. Cloutier, et al. 2012. A molecular roadmap of reprogramming somatic cells into iPS cells. *Cell.* 151:1617–1632. https://doi.org/10.1016/j.cell.2012.11.039

Preker, P., J. Nielsen, S. Kammler, S. Lykke-Andersen, M.S. Christensen, C.K. Mapendano, M.H. Schierup, and T.H. Jensen. 2008. RNA exosome depletion reveals transcription upstream of active human promoters. *Science.* 322:1851–1854. https://doi.org/10.1126/science.1164096

Quinlan, A.R., and I.M. Hall. 2010. BEDTools: a flexible suite of utilities for comparing genomic features. *Bioinformatics.* 26:841–842. https://doi.org/10.1093/bioinformatics/btq033

Quintero-Ronderos, P., and P. Laissue. 2018. The multisystemic functions of FOXD1 in development and disease. *J. Mol. Med. (Berl.).* 96:725–739. https://doi.org/10.1007/s00109-018-1665-2

Reid, C.D., A.B. Steiner, S. Yaklichkin, Q. Lu, S. Wang, M. Hennessy, and D.S. Kessler. 2016. FoxH1 mediates a Grg4 and Smad2 dependent transcriptional switch in Nodal signaling during Xenopus mesoderm development. *Dev. Biol.* 414:34–44. https://doi.org/10.1016/j.ydbio.2016.04.006

Santoni, F.A., J. Guerra, and J. Luban. 2012. HERV-H RNA is abundant in human embryonic stem cells and a precise marker for pluripotency. *Retrovirology.* 9:111. https://doi.org/10.1186/1742-4690-9-111

Schneider, C., G. Kudla, W. Wlotzka, A. Tuck, and D. Tollervey. 2012. Transcriptome-wide analysis of exosome targets. *Mol. Cell.* 48:422–433. https://doi.org/10.1016/j.molcel.2012.08.013

Schoenberg, D.R., and L.E. Maquat. 2012. Regulation of cytoplasmic mRNA decay. *Nat. Rev. Genet.* 13:246–259. https://doi.org/10.1038/nrg3160

Sigova, A.A., A.C. Mullen, B. Molinie, S. Gupta, D.A. Orlando, M.G. Guenther, A.E. Almada, C. Lin, P.A. Sharp, C.C. Giallourakis, and R.A. Young. 2013. Divergent transcription of long noncoding RNA/mRNA gene pairs in embryonic stem cells. *Proc. Natl. Acad. Sci. USA.* 110:2876–2881. https://doi.org/10.1073/pnas.1221904110

Szutorisz, H., A. Georgiou, L. Tora, and N. Dillon. 2006. The proteasome restricts permissive transcription at tissue-specific gene loci in embryonic stem cells. *Cell.* 127:1375–1388. https://doi.org/10.1016/j.cell.2006.10.045

Tarn, W.Y., and J.A. Steitz. 1997. Pre-mRNA splicing: the discovery of a new spliceosome doubles the challenge. *Trends Biochem. Sci.* 22:132–137. https://doi.org/10.1016/S0968-0004(97)01018-9

Teo, A.K., S.J. Arnold, M.W. Trotter, S. Brown, L.T. Ang, Z. Chng, E.J. Robertson, N.R. Dunn, and L. Vallier. 2011. Pluripotency factors regulate definitive endoderm specification through eomesodermin. *Genes Dev.* 25:238–250. https://doi.org/10.1101/gad.607311

Thomson, J.A., J. Itskovitz-Eldor, S.S. Shapiro, M.A. Waknitz, J.J. Swiergiel, V.S. Marshall, and J.M. Jones. 1998. Embryonic stem cell lines derived from human blastocysts. *Science.* 282:1145–1147. https://doi.org/10.1126/science.282.5391.1145

Tomecki, R., M.S. Kristiansen, S. Lykke-Andersen, A. Chlebowski, K.M. Larsen, R.J. Szczesny, K. Drazkowska, A. Pastula, J.S. Andersen, P.P. Stepien, et al. 2010. The human core exosome interacts with differentially localized processive RNases: hDIS3 and hDIS3L. *EMBO J.* 29:2342–2357. https://doi.org/10.1038/emboj.2010.121

Trapnell, C., B.A. Williams, G. Pertea, A. Mortazavi, G. Kwan, M.J. van Baren, S.L. Salzberg, B.J. Wold, and L. Pachter. 2010. Transcript assembly and quantification by RNA-Seq reveals unannotated transcripts and isoform switching during cell differentiation. *Nat. Biotechnol.* 28:511–515. https://doi.org/10.1038/nbt.1621

Tseng, C.K., H.F. Wang, A.M. Burns, M.R. Schroeder, M. Gaspari, and P. Baumann. 2015. Human telomerase RNA processing and quality control. *Cell Reports.* 13:2232–2243. https://doi.org/10.1016/j.celrep.2015.10.075

Wang, Y., S. Baskerville, A. Shenoy, J.E. Babiarz, L. Baehner, and R. Blelloch. 2008. Embryonic stem cell-specific microRNAs regulate the G1-S transition and promote rapid proliferation. *Nat. Genet.* 40:1478–1483. https://doi.org/10.1038/ng.250

Weick, E.M., M.R. Puno, K. Januszyk, J.C. Zinder, M.A. DiMattia, and C.D. Lima. 2018. Helicase-Dependent RNA Decay Illuminated by a Cryo-EM Structure of a Human Nuclear RNA Exosome-MTR4 Complex. *Cell.* 173:1663–1677.

Yamamoto, M., C. Meno, Y. Sakai, H. Shiratori, K. Mochida, Y. Ikawa, Y. Saijoh, and H. Hamada. 2001. The transcription factor FoxH1 (FAST) mediates Nodal signaling during anterior-posterior patterning and node formation in the mouse. *Genes Dev.* 15:1242–1256. https://doi.org/10.1101/gad.883901

Young, R.A. 2011. Control of the embryonic stem cell state. *Cell.* 144:940–954. https://doi.org/10.1016/j.cell.2011.01.032

Zinder, J.C., and C.D. Lima. 2017. Targeting RNA for processing or destruction by the eukaryotic RNA exosome and its cofactors. *Genes Dev.* 31:88–100. https://doi.org/10.1101/gad.294769.116